A CMOS Analog Front-End Circuit for Micro-Fluxgate Sensors

by

Karthik Pappu

A Thesis Presented in Partial Fulfillment
of the Requirements for the Degree
Master of Science

Approved August 2013 by the
Graduate Supervisory Committee:

Bertan Bakkaloglu, Chair
Jennifer Blain Christen
Hongbin Yu

ARIZONA STATE UNIVERSITY

December 2013

ABSTRACT

Fluxgate sensors are magnetic field sensors that can measure DC and low frequency AC magnetic fields. They can measure much lower magnetic fields than other magnetic sensors like Hall effect sensors, magnetoresistive sensors etc. They also have high linearity, high sensitivity and low noise. The major application of fluxgate sensors is in magnetometers for the measurement of earth's magnetic field. Magnetometers are used in navigation systems and electronic compasses. Fluxgate sensors can also be used to measure high DC currents. Integrated micro-fluxgate sensors have been developed in recent years. These sensors have much lower power consumption and area compared to their PCB counterparts. The output voltage of micro-fluxgate sensors is very low which makes the analog front end more complex and results in an increase in power consumption of the system.

In this thesis a new analog front-end circuit for micro-fluxgate sensors is developed. This analog front-end circuit uses charge pump based excitation circuit and phase delay based read-out chain. With these two features the power consumption of analog front-end is reduced. The output is digital and it is immune to amplitude noise at the output of the sensor. Digital output is produced without using an ADC. A SPICE model of micro-fluxgate sensor is used to verify the operation of the analog front-end and the simulation results show very good linearity.

ACKNOWLEDGMENTS

I am very grateful to my advisor and committee chair Dr. Bertan Bakkaloglu for his guidance, encouragement and patience. He is the source of my inspiration. I would like to give special appreciation to Dr. Jennifer Blain Christen and Dr. Hongbin Yu for being a part of my thesis defense committee.

I am thankful to my project mates Mr. Koushik Malladi, Mr. Abhiram Mummareddy, Mr. Vivek Parasuram, Mr. Amit Kumar, Mr. Navankur Beohar and Mr. Chao Fu for their support, knowledge sharing and interactive discussions.

I would like to thank Mr. James Laux for his support regarding software. I would also like to thank all my professors for their knowledge sharing during my course work.

I am thankful to my parents, sister and my family for their support and encouragement. I would like to thank all my friends for their support and friendship.

TABLE OF CONTENTS

Page

CHAPTER Page

LIST OF TABLES

Table Page

LIST OF FIGURES

Figure Page

Figure Page

Chapter 1
INTRODUCTION

1.1 Background

Fluxgate sensors are magnetic sensors that can measure DC and low frequency AC magnetic fields. They are capable of measuring magnetic fields order of nT to one mT with resolution as low as 10pT [1]. They are also sensitive to the direction of magnetic field. These sensors have very high linearity, sensitivity, low noise and ruggedness. They can measure much lower magnetic fields than other magnetic field sensors like Hall sensors, magnetoresistive sensors, search coil magnetometers etc. with good linearity. SQUIDs (super conducting quantum interference devices) are the only magnetic sensors which have higher sensitivity than fluxgate sensors and they are very expensive.

The following are a few important applications of fluxgate sensors [2] [3] [4] [7].

- Earth magnetic field measurement in magnetometers for navigation systems and electronic compasses
- Detection of minerals and ores
- Space Magnetometers
- Measurement of DC and low frequency AC currents
- Mechanical measurements such as linear and angular position, displacement and velocity etc.

1.2 Research Goals

Conventional PCB fluxgate sensors consume a large amount of area and power which limits the application of these sensors. Low power, low area micro-fluxgate sensors are developed over the past few years increasing the possibility of realizing magnetic micro systems.

One of the major challenges of integrated micro-fluxgate sensors is the realization of magnetic core. Micro-fluxgate sensors are mostly realized either in a CMOS process where the magnetic core is realized using post processing [5] - [7] or using MEMS processes [8] [9] [12].

Although micro-fluxgate sensors offer great savings in area and power they produce much lower outputs compared to the traditional PCB fluxgate sensors. This makes the analog front-end circuit for micro-fluxgate sensors to be more complex and it also consumes more power. Portable devices and wireless sensor networks require low power sensor systems. Hence along with a reduction of power of the sensor it is important to realize low power analog front end circuits.

The goal of this thesis is to address to develop a new low power analog front-end circuit for micro-fluxgate sensors which has the following properties

- Low power
- ADC free digital output
- Produces an output that varies linearly with external magnetic field
- Can be integrated with other CMOS circuits

1.3 Operating Principle of Fluxgate Sensor

The fluxgate sensor consists of an excitation coil, a sensing coil and a magnetic core. The current through the excitation coil should be high enough to saturate the core in one direction or the other twice per each cycle. When the core is not saturated it offers a low reluctance path to the external magnetic field and when the core is saturated it offers a high reluctance path to the external magnetic field, there by gating the external flux. Hence the sensor is called a fluxgate. This change in flux induces a voltage in the sensing coil [10].

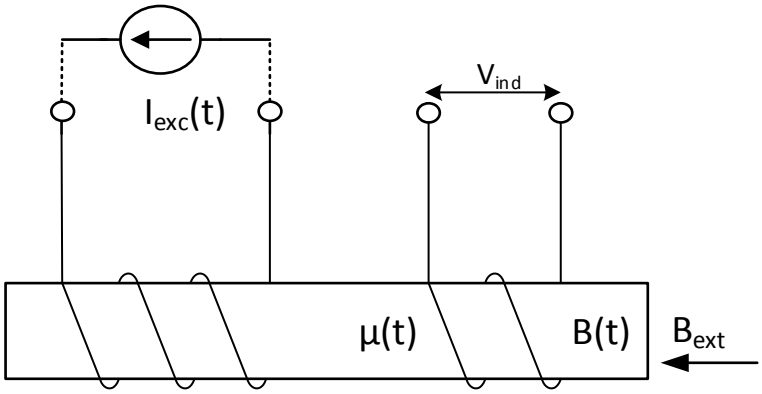

Figure 1.1 Basic Fluxgate Sensor Principle

1.4 Second Harmonic Principle

The second harmonic of the output voltage across the sensing coil of a fluxgate sensor is proportional to the external magnetic field [11]. If a sinusoidal current of frequency $\omega/2\pi$ is used to excite the fluxgate sensor it creates a magnetic field H_{ref} given by equation (1.1). The external magnetic field Hext will be added to this.

$$H_{ref} = H_{refmax} \sin\omega t \qquad (1.1)$$

If N is the demagnetization factor and μ is the relative permeability, the magnetic field within the core is given by:

$$H_{int} = \frac{H_{ext} + H_{refmax} \sin\omega t}{1 + N(\mu_r - 1)} \tag{1.2}$$

This magnetic field is normalized to H_0* which is given as:

$$H_0^* = \frac{2}{\pi} \frac{B_{sat}[1 + N(\mu_r - 1)]}{\mu_r \mu_0} \tag{1.3}$$

The normalized magnetic field strength within the core is given by:

$$h_{int} = \frac{H_{int}}{H_0^*} = h_{ext} + h_{refmax} \sin\omega t \tag{1.4}$$

The magnetization curve can be approximated by a normalized third order polynomial as:

$$b(h) = a_1 h - a_3 h^3 \tag{1.6}$$

$$b(h) = a_1 h_{ext} + a_1 h_{refmax} \sin\omega t - a_3 (h_{ext} + h_{refmax} \sin\omega t)^3 \tag{1.7}$$

where b is the normalized flux density

The output voltage across the sensing coil is given as:

$$V_{out} = -N \frac{d\phi}{dt} = -NA \frac{dB}{dt} \tag{1.8}$$

where N is the number of turns of the sensing coil and A is the area of cross section of the magnetic core.

The normalized output voltage is given as:

$$v_{out} = -\frac{V_{out}}{NA} = \frac{dB}{dt} = B_0 \frac{dB}{dt} \tag{1.9}$$

$$\begin{aligned} v_{out} = B_0\omega(a_1 h_{ref\,max} - 3a_3 h_{ext}^2 h_{ref\,max}^2 - 0.75a_3 h_{ref\,max}^3)\cos\omega t + \\ 3B_0\omega a_3 h_{ext} h_{ref\,max}^2 \sin 2\omega t + 0.75B_0\omega a_3 h_{ref\,max}^3 \cos 3\omega t \end{aligned} \tag{1.10}$$

The second-harmonic component of the voltage across the sensing coils is given as:

$$V_{out\,2h} = -3B_0 NA\omega a_3 h_{ext} h_{ref\,max}^2 \sin 2\omega t \tag{1.11}$$

Given that all other factors are constant the amplitude of second harmonic is proportional to the external magnetic field strength.

1.5 Ring-type Fluxgate Sensor

It can be seen from equation (1.10) that the output of the sensor also contains DC and first harmonic contents and hence it would require a bandpass filter to extract the second harmonic. A ring-type fluxgate sensor [12] would produce an output that does not contain the DC and first harmonic components. The output now contains only the even harmonics. Therefore the second harmonic can be obtained by low-pass filtering. It would also reduce the current required to saturate the magnetic core because the flux is now flowing in a closed path.

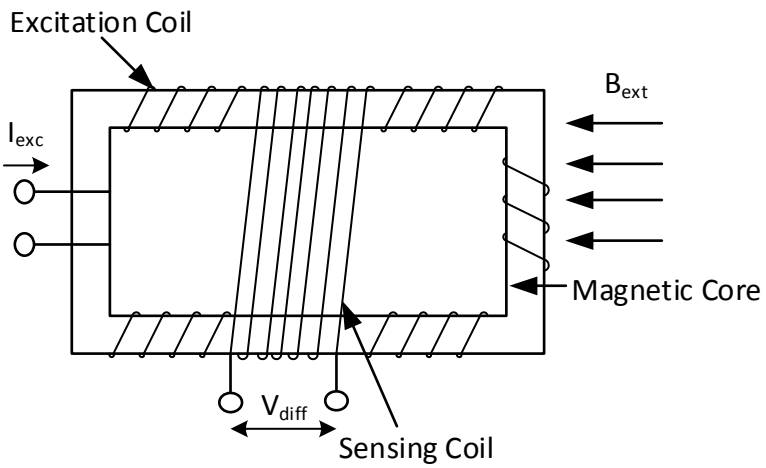

Figure 1.2 Ring-type Fluxgate Sensor

The sensitivity of a ring-type sensor is twice that of a single core sensor as the output voltage is now proportional to the difference in magnetic fields between the two portions of the core.

1.6 Phase Delay Principle

Phase delay technique is based on the observation that the external magnetic field information is carried by the phase difference between two consecutive pulses at the output of the fluxgate sensor [10] [19]. The output of a single core single sensing coil fluxgate sensor for triangular excitation signal is shown in Figure (1.3). It can be seen that in presence of external magnetic field the phase delay between consecutive pulses which is given as t_2-t_1 increases. A counter is set and reset such that it measures this phase delay. The counter is run on a clock with a time period of T_s which is smaller than the time period of excitation current T_0. If H_{ext} is the external magnetic field strength and H_m is the peak value of the magnetic field strength due to excitation current, then for a triangular excitation signal the difference between t_2 and t_1 is given as:

$$t_2 - t_1 = \Delta T = \frac{T_0 . H_{ext}}{2H_m} \tag{1.12}$$

The counter output N_s is given by:

$$N_s = \frac{T_0 . H_{ext}}{2T_s . H_m} \tag{1.13}$$

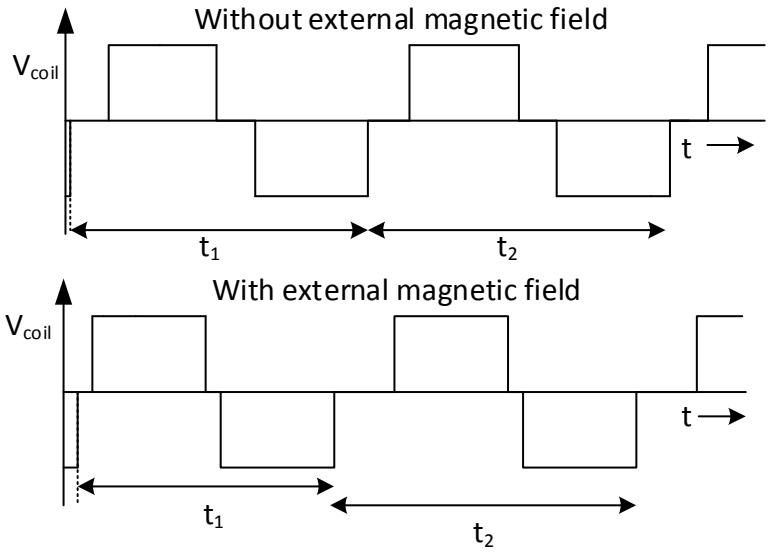

Figure 1.3 Output of a Single Core Fluxgate Sensor

The output waveforms for a ring-type sensor with triangular excitation signal are shown in Figure (1.4). It can be seen that the phase delay t_2-t_1 transforms into the pulse width of the output voltage across the sensing coils. The sensitivity of the sensor is also doubled because the difference in magnetic field strengths associated with the respective portions of the core is now twice the external magnetic field. The output of a ring-type sensor is given as:

$$\Delta T = \frac{T_0 . H_{ext}}{H_m} \tag{1.14}$$

$$N_s = \frac{T_0 . H_{ext}}{T_s . H_m} \tag{1.15}$$

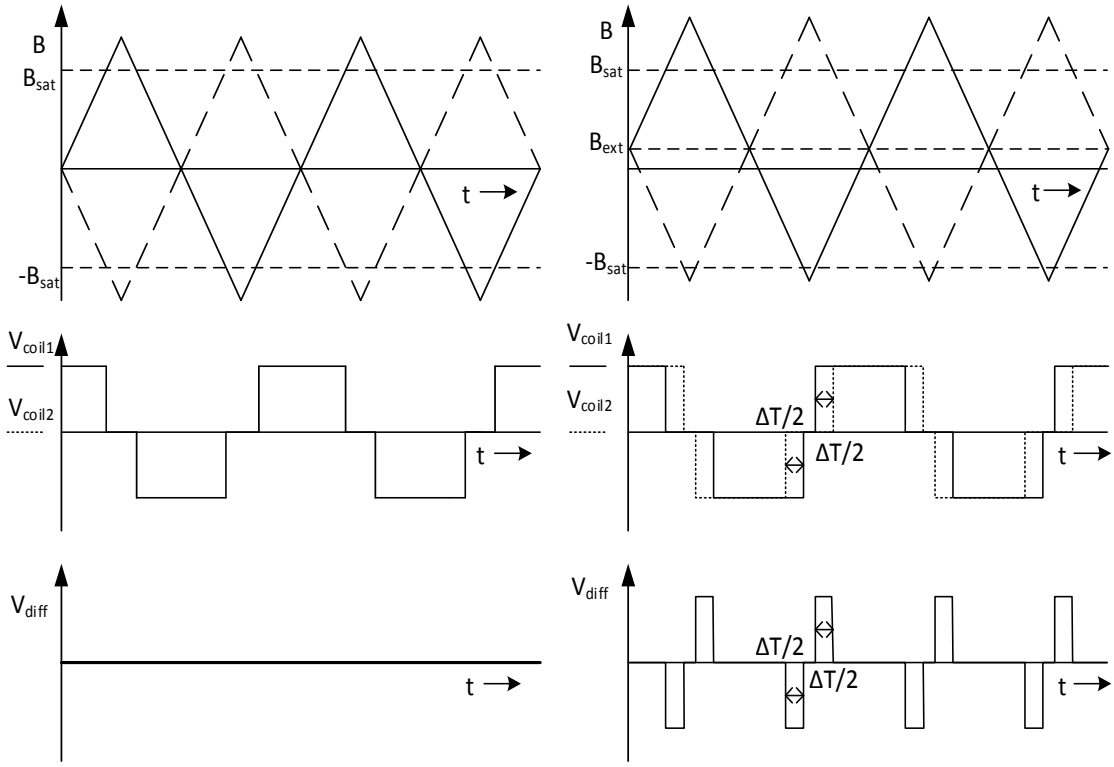

Figure 1.4 Output of a Ring-type Fluxgate Sensor

The advantages of a phase delay based read-out are listed below.

1) The output of the sensor is available in digital form
2) The output is independent of the area of cross section of the core
3) Cross-field effect is expected to be negligible, because the response is theoretically independent of H_c and H_r when the loop remains symmetric within an excitation cycle.

4) The receiving coil properties do not influence the sensor's output considerably as long as the output voltage has amplitude greater than the noise floor. Hence coils of inferior characteristics such as integrated coils can be used for fabricating the sensor.

1.7 Miniature Fluxgate Magnetic Sensors

Miniaturization of fluxgate sensors enables the generation of micro-fluxgate magnetic sensors that are cost effective, low power and have low area. Applications such as current sensing, navigation systems and portable devices demand smaller fluxgate sensors. Micro-fluxgate sensors can be integrated with the analog front end circuitry and also other CMOS circuits and ASICs. The traditional fluxgate sensors have wound excitation and sensing coils whose cost can be reduced using micro fabrication techniques. The sensitive parts like the magnetic core are generally realized by post-processing. The low power micro-fluxgate sensors integrated with other CMOS circuits can be a part of smart sensor systems. Several state of the art micro-fluxgate sensors fabricated using different processes are described in [5]-[9].

A ring-type micro-machined fluxgate sensor fabricated in UV-LIGA process has been reported in [12]. Instead of saturating the entire core only a part of the core where the sensing coil is placed is saturated by reducing the area of the core in these portions. Hence the peak value of excitation current required to saturate the core reduced to 50mA from 250mA. The peak to peak value of output voltage is around 30mV. A sensitivity of 389V/T has been obtained.

A comparison between a double axis PCB fluxgate sensor and an IC version is made in [5]. The coils for the micro-fluxgate sensor have been fabricated in 0.5μm

CMOS technology and the ferromagnetic core is deposited using post processing. The micro-fluxgate sensor yielded a 75% saving in area with respect to a direct scaling of the PCB version. The IC version also showed a tremendous decrease in power consumption. It required only 5mA peak current to saturate the core compared to 600mA of the PCB fluxgate sensor. This shows that a great reduction in power and area can be obtained using micro-fluxgate sensors.

While the micro-fluxgate sensors work at lower power and area they have decreased sensitivity and more noise [5] [10]. The voltage across a coil wrapped around a magnetic core excited by a sinusoidal current is given as:

$$V_{ind} = -\frac{d\Phi}{dt} = -N_{sense} * S * \frac{d}{dt}\left(\frac{\mu * N_{exc} * I_0.\sin(2\pi f_{exc} t)}{l_m}\right) \qquad (1.16)$$

where N_{sense} is the number of turns in the sensing coil, S is the cross section area of the core, μ is the absolute magnetic permeability, N_{exc} is the number of turns in the excitation coil, I_0 is the amplitude of excitation current, f_{exc} is the excitation frequency and l_m is the length of the magnetic path. Because of the area reduction the amplitude of the sensed signal and hence the sensitivity of the sensor decrease with miniaturization. Due to this reason the micro-fluxgate sensors are usually operated at much higher frequencies than PCB sensors to get a voltage signal of amplitude good enough to be processed by the read out circuitry. For example the PCB sensor in [5] works with an excitation frequency of 10KHz and produces an output with 15mV amplitude where as the IC version of it works at an excitation frequency of 100KHz and produces an output with 1mV amplitude. Micro-fluxgate sensors also have higher noise than that of PCB sensors.

1.8 SPICE Model of Micro fluxgate Sensor

It is important to test the analog front-end circuit with a valid model of micro-fluxgate sensor before fabrication. A SPICE model for micro-fluxgate sensor is presented in [12]. The fabrication results match with the simulation results using this model. This SPICE model is used to verify the operation of the developed analog front-end circuit. The magnetic core is modeled using a current source, resistors and diodes. The model for magnetic core is shown in Figure (1.5).

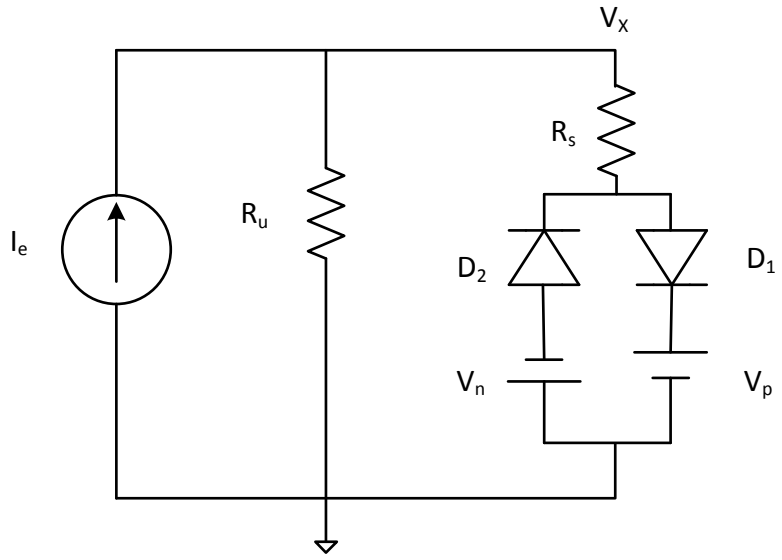

Figure 1.5 SPICE Model of Magnetic Core

Ie is a current controlled current source which corresponds to the magnetic field intensity (H). The voltage V_x corresponds to the magnetic flux density (B). R_u is proportional to the permeability of the core in non-saturation region and R_s is proportional to the permeability in the saturation region. The B-H curve is shown in Figure (1.6). If I_e increases in positive direction the voltage V_x also increases. The slope of the V-I curve in this region is equal to R_u. After the point A the diode D_1 becomes forward biased and the core becomes saturated.

Now if the current I_e is decreased the core remains in saturation till the point C. After this point the core comes out of saturation and both the diodes are reverse biased. The curve follows the path CDE. The slope of the V-I curve is again R_u. The current through the reverse biased junction of the diodes flows from V_x to ground and hence V_x will stay positive even if Ie is zero. Similarly V_x will be negative in the opposite direction even if Ie is zero. The curve follows the path GAB. Thus this model can simulate both hysteresis and saturation phenomenon in magnetic cores.

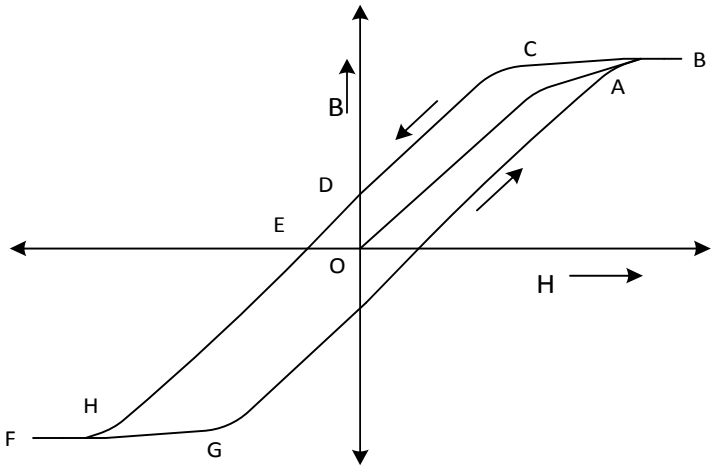

Figure 1.6 B-H Curve

The sensor model for ring-type sensor is shown in Figure (1.7). The excitation circuit consists of a current source I_{exc} in series with an excitation coil with a resistance R_{exc} and inductance L_{exc}. This produces a magnetic field of intensity H_{exc} given by:

$$H_{exc} = \frac{N_{exc} * I_{exc}}{L_m} \qquad (1.17)$$

N_{exc} is the number of turns in the excitation coil. I_{exc} is the excitation current and L_m is the magnetic length of the core. The external field is modeled as two current

sources H_{ext}. So the magnetic field strength in one arm is $H_{exc}+H_{ext}$ and the magnetic field in the other arm is $H_{exc}-H_{ext}$.

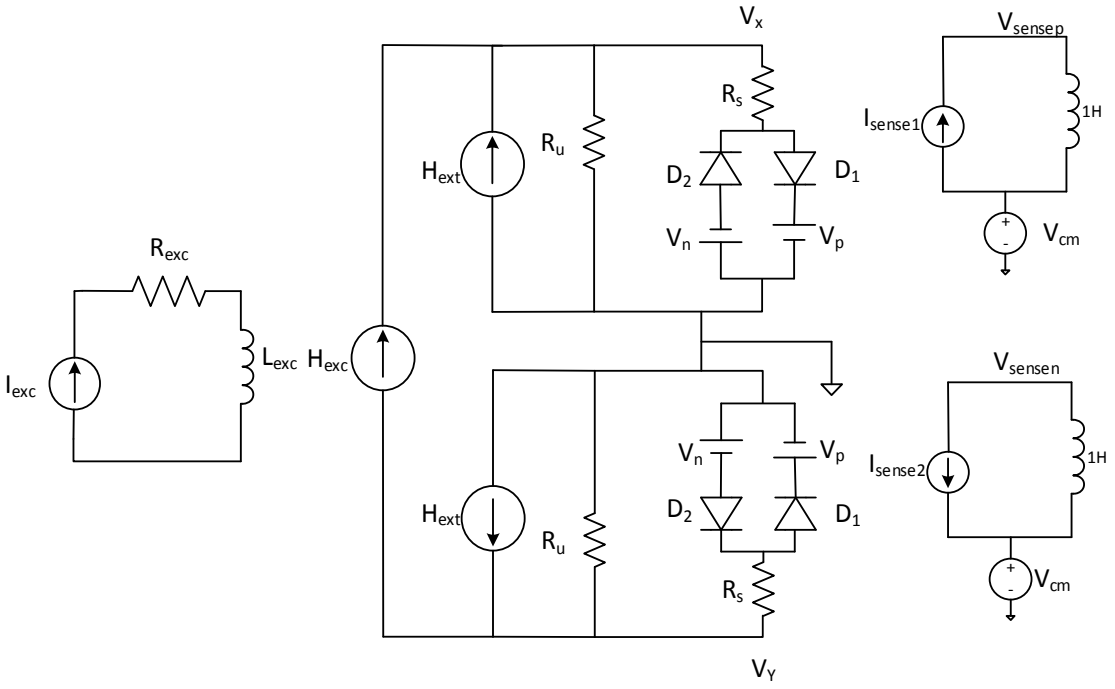

Figure 1.7 SPICE Model of Fluxgate Sensor

$$I_{sense1} = N_{sense} * A_c * V_X \tag{1.18}$$

$$I_{sense2} = N_{sense} * A_c * V_Y \tag{1.19}$$

I_{sense1} and I_{sense2} are voltage controlled current sources with gain proportional to $N_{sense}*A_c$, where N_{sense} is the number of turns in the sensing coils and A_c is the area of cross section of the core. V_{cm} sets the common mode dc voltage at the output of the sensing coils. The currents $I_{sense1,2}$ are passed through inductors to produce the final output voltages.

$$V_{sense1} = N_{sense} * \frac{d\phi}{dt} = N_{sense} * A_c * \frac{dV_x}{dt} \tag{1.20}$$

$$V_{sense2} = N_{sense} * \frac{d\phi}{dt} = N_{sense} * A_c * \frac{dV_Y}{dt} \quad (1.21)$$

This sensor model has been tested with the fabricated micro-fluxgate sensors in [13]. The results show good matching between the simulated and measured outputs. Hence this model is used in this thesis. The parameters of the sensor fabricated in [13] are shown in Table 1.1 below.

Parameter	**Value**
Number of turns in excitation coil (N_{exc})	44
Number of turns in sensing coils (N_{sense})	14
Resistance of Excitation coil (R_{exc})	3Ω
Inductance of Excitation coil (L_{exc})	1.01μH
Length of the magnetic path (L_m)	700μm
Area of cross section (A_c)	700μm*100μm
Excitation Frequency	50KHz
Peak value of excitation current	50mA

Table 1.1 Parameters of Ring-type Micro-Fluxgate Sensor

Chapter 2

STATE-OF-THE-ART ANALOG FRONT-END CIRCUITS

Traditional fluxgate sensors are excited using sinusoidal or pulse excitation [14]. Sinusoidal excitation provides low noise signals where as pulsed excitation is easier to implement. Triangular excitation gives lower noise than pulse excitation and is easier to implement compared to sinusoidal excitation [15]. Hence triangular excitation is most suited for integrated fluxgate sensors. In this section a review of the existing state of the art analog front-end circuits for micro fluxgate sensors are presented.

2.1 A CMOS Front-End Circuit for Integrated Fluxgate Sensors

The analog front-end circuit presented in [15] contains an excitation circuit, a timing unit and a read-out unit. A 400KHz clock is divided internally to get a 100KHz clock and 200KHz clock. The 100KHz clock is used in the excitation circuit to generate a triangular voltage signal at 100KHz. The 200KHz clock is used to demodulate the output of the fluxgate sensor. It is essential that these two clocks have a 50% duty cycle to ensure proper demodulation.

A schematic of the excitation circuit is shown in Figure (2.1). It consists of an integrator followed by a transconductance amplifier. The resistor and capacitor are on chip but the input to the integrator $\pm V_{in}$ is external. This makes it possible to use the system for sensors with different saturation current requirement. For one half of the clock period of 100KHz clock the input is connected to $+V_{in}$ and for the other half it is connected to $-V_{in}$. This produces a triangular voltage wave around zero at the output of the integrator. This triangular voltage is fed to a transconductance amplifier which produces a triangular current. This current is passed through a current mirror into a class

AB output stage. The voltages V_{bias1} and V_{bias2} are internal. The output stage has a supply voltage of 5V and the other circuits have a supply voltage of 3.3V.

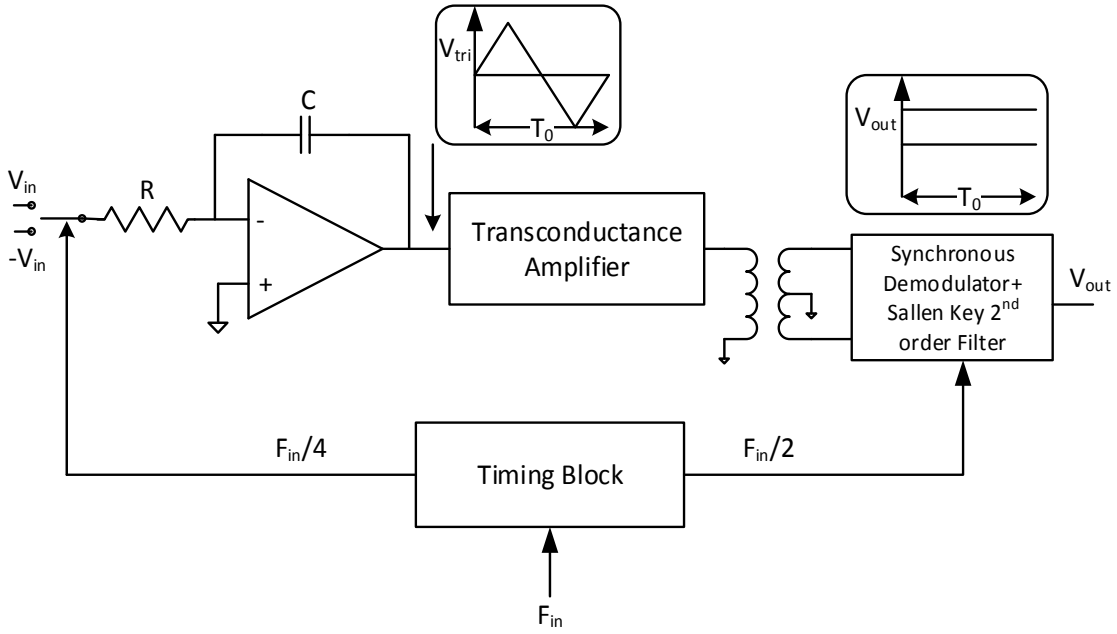

Figure 2.1 A CMOS Front-End Circuit for Integrated Fluxgate Sensors

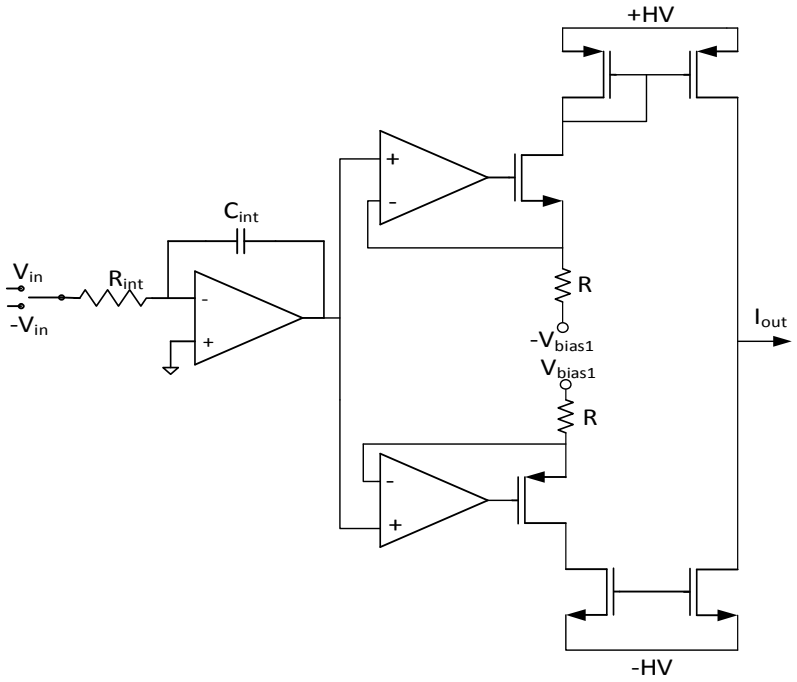

Figure 2.2 Excitation Circuit

Second harmonic principle is used to obtain the output signal. The read-out circuit has a synchronous demodulation unit followed by a second order Sallen-Key low pass filter to extract the second harmonic component of the output of the fluxgate sensor.

Some of the important specifications of this analog front-end circuit are listed in Table (2.1). These results are obtained by testing the analog front end on a PCB fluxgate sensor.

Process	0.35μm, 2 poly, 5 metal
Sensitivity	920V/T
Range	±60μT
Linearity	6 % F.S
Power Consumption	42 mW @ 5V 8mW @ 3.3V
Area without pads	1700*350μm^2

Table 2.1 Key Specifications

The major disadvantage of this analog front end circuit is the use of symmetric power supply for the generation of triangular current in both positive and negative directions. Current CMOS technologies do not use symmetric power supplies and hence it would be difficult to integrate this analog front-end circuit with other CMOS circuits and ASICs. Also it does not provide the output in digital format.

2.2 A CMOS 2D Micro-fluxgate Earth Magnetic Field Sensor

A double axis micro-fluxgate sensor with its analog front-end circuit has been presented in [7] and [16]. A 0.5μm CMOS process followed by post processing for the magnetic core is used to fabricate the micro-fluxgate sensor. A new technique called dc-magnetron sputtering is used which allows us to get a ferromagnetic core of good

properties with a lower thickness. The excitation coil has a resistance of 123.4Ω. The sensor needs to be excited with a 100 kHz signal and requires 18mA of current to saturate the core. The differential peak to peak voltage is 3.5mV which is amplified by 33dB before it is processed by the read-out chain.

The excitation and read-out circuits are shown in Figure (2.3). The excitation circuit has two blocks- one at 3.3V and one at 26V. The 3.3V block generates a square wave of 100 kHz with an amplitude set by the external voltage V_{in}. The square wave is integrated to obtain a triangular waveform around mid supply range. The 26V block consists of an operational amplifier with low-impedance class AB output stage. The class AB output stage provides all the current required for the micro-fluxgate sensor. A decoupling stage is used between the 3.3V and 26V blocks.

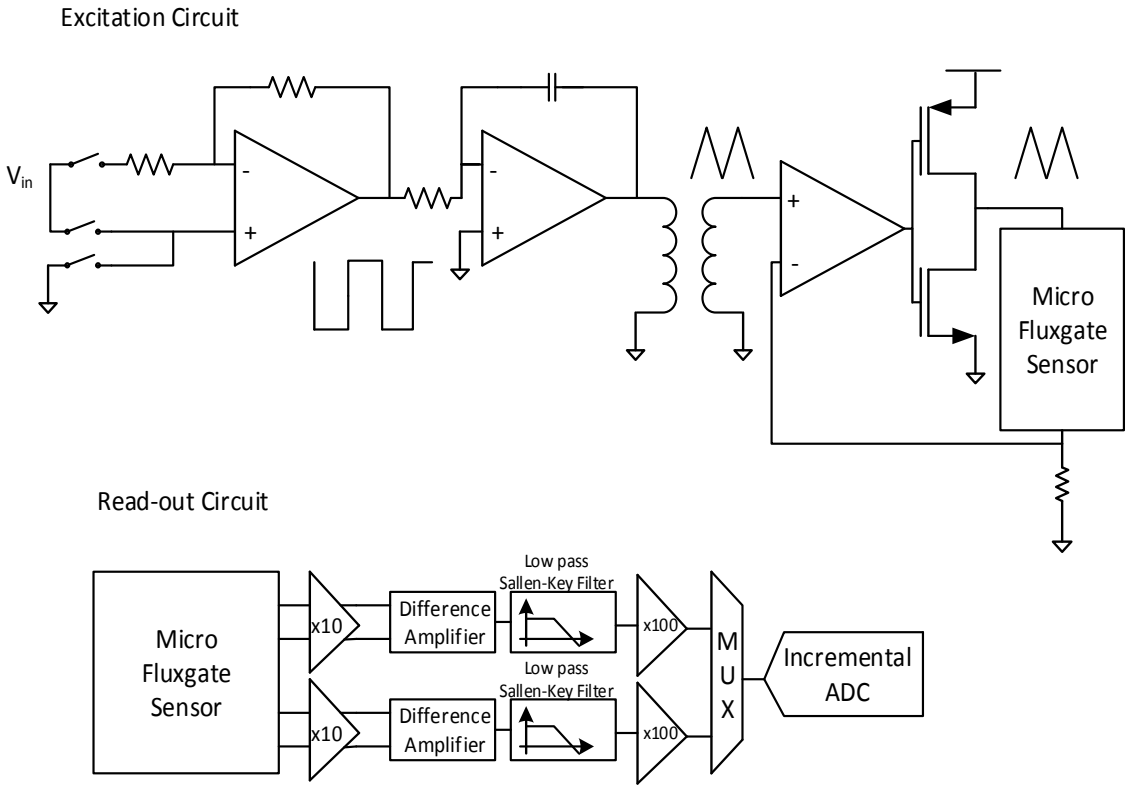

Figure 2.3 CMOS 2D Micro-Fluxgate Earth Magnetic Field Sensor

The differential output voltage is amplified by a factor of 10 and then passed through a difference amplifier that amplifies the difference between the two outputs of the sensing coils. A Sallen- Key filter is used to extract the second harmonic component of the output voltage. The output of the Sallen- Key filter is amplified further before being digitized by a 13bit incremental ADC. The salient features of this analog front end circuit are provided in Table (2.2).

Sensor Technology	0.5μm CMOS
Ferromagnetic Core	Vitrovac 6025 X deposited by DC-magnetron sputtering
Interface circuit technology	0.35μm CMOS
Sensor Area	$3.2mm^2$
Interface circuit area	$1.7mm^2$
Supply Voltage	3.3V-26V
Power consumption of sensor	13.7mW
Power consumption of system	90mW
Magnetic field range	±60μT
Linearity Error	3% of full scale
Angle Error (Earth Magnetic Field)	4^o

Table 2.2 Key Specifications

This analog front-end also uses symmetric power supply to generate the triangular current in both positive and negative directions and hence it would be difficult to integrate it with other CMOS circuits. Also the power consumption for the analog front end is around 76.3mW which is very high. In addition to these the use of a decoupling stage increases the cost of the interface circuit.

2.3 Low-voltage Fluxgate Sensor Interface Circuit

A low-voltage fluxgate magnetic sensor interface circuit with digital output for portable applications is presented in [17]. Two different excitation circuits have been proposed. The excitation circuit that works at a relatively lower voltage of 3.3V is shown in Figure (2.4). It consists of an H- bridge which changes the direction of current through the excitation coil of the fluxgate sensor at the desired frequency thus eliminating the use of split power supply. The 3.3V excitation circuit uses an external inductance of 380μH to generate the triangular current waveform.

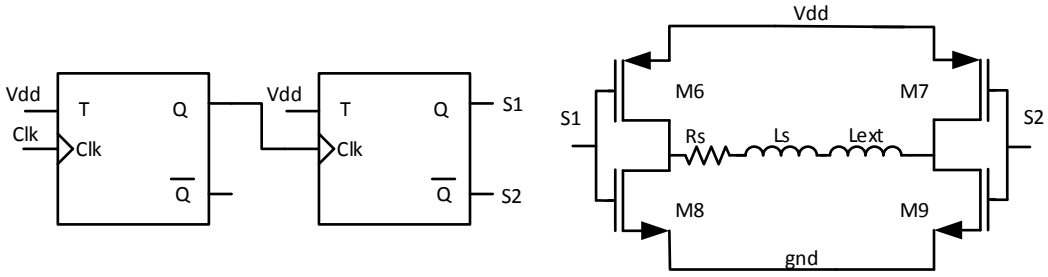

Figure 2.4 3.3V Excitation Circuit

The excitation circuit with 5V power supply has a triangular voltage generator, a voltage to current converter and an H-bridge. A square wave is generated and then integrated using an active integrator to obtain a triangular wave. This triangular voltage is level shifted and converted into triangular current by using a voltage to current converter. The current is mirrored using a cascode current mirror to get a 20mA peak current. The peak value of the triangular current can be modified by changing the reference voltage Vref which is set externally. The H-bridge is driven by signals S1 and S2 to switch alternatively the current flowing into the excitation coil of the sensor. This would allow the sensor to be excited with a 40mA peak to peak current without using symmetric supply voltage.

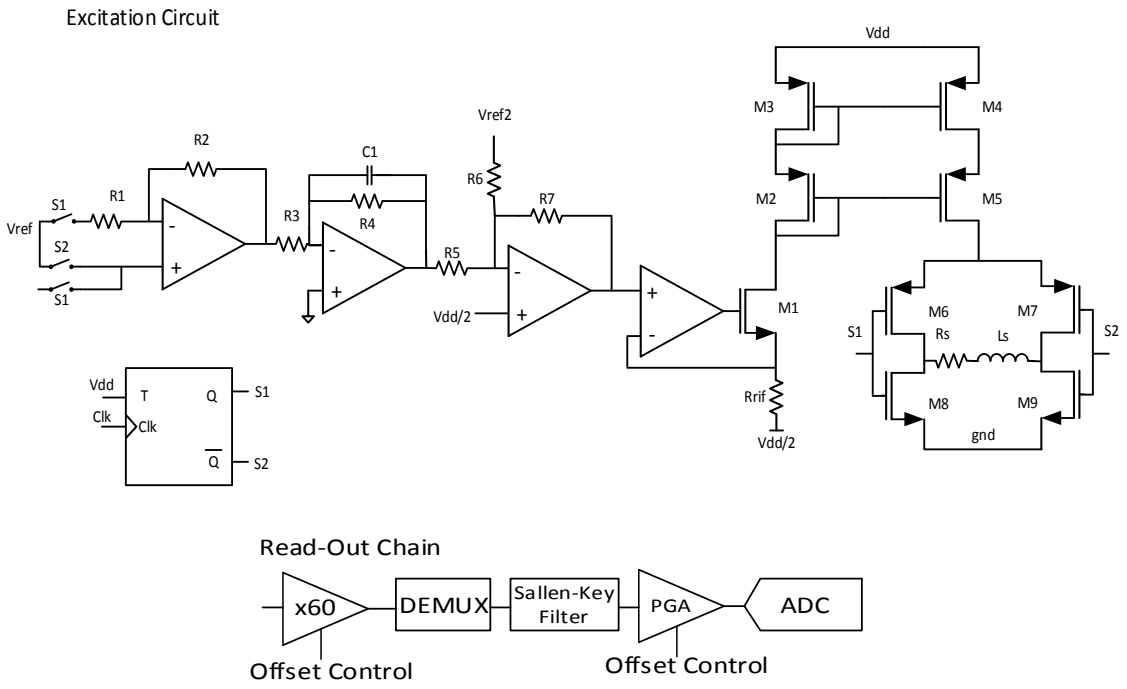

Figure 2.5 5V Excitation Circuit and Read-Out Chain

The read-out chain presented is shown in Figure (2.5). It performs a synchronous demodulation to obtain the extract the second harmonic component in the output of the fluxgate sensor. The difference in the outputs of the sensing coils is amplified by 35dB using an instrumentation amplifier. Each operational amplifier used in the instrumentation amplifier consumes 168μW of power. The single ended output is demodulated using a coherent orthogonal demodulator. The demodulation is done at a frequency of 200KHz. A quadrature demodulator is used. The output of the demodulator is passed through a Sallen- Key filter that produces a dc signal proportional to the second harmonic component of the output voltage. The dc signal is amplified by a programmable gain amplifier (PGA) before it is digitized by a 13 bit incremental ADC. The total power consumed by the interface circuit and its area are not mentioned.

Chapter 3

ANALOG FRONT-END ARCHITECTURE

A review of the existing state-of-the-art analog front end circuits for micro-fluxgate sensors presented in chapter 2 reveals that triangular excitation signal is preferred as it gives good noise performance and is easier to generate. The proposed analog front end circuit uses a charge pump based excitation circuit to generate the triangular excitation current. The advantages of using phase delay technique to extract the output signal in digitized form have been listed in section 1.6. The proposed analog front-end circuit uses phase delay technique in the read-out chain.

The developed analog front-end architecture is shown in Figure (3.1) and Figure (3.2). The excitation circuit consists of a charge pump which charges and discharges an external capacitor CSET linearly to produce a triangular voltage waveform at its output. This is done by alternatively turning on two constant current sources I_p and I_n. When the clock goes low the capacitor CSET is charged through a constant current source I_p. When the clock goes high the capacitor is discharged through the constant current source I_n. This generates a triangular voltage at the output of the charge pump. The charge pump works on a 100KHz clock. The triangular voltage is periodically reset to a fixed dc value so as to provide a proper input common mode to the next stage.

The triangular voltage waveform generated by the charge pump is converted into a triangular current by a voltage to current converter. The triangular voltage is applied through a feedback loop across an external resistor RSET whose negative terminal is held constant at a dc voltage V_{sink}. The external resistor sets the current in this branch. A current sink with very low output impedance is used to set the voltage at the negative

terminal of the resistor RSET to a known dc value V_{sink}. Since the triangular voltage at the output of the charge pump is reset to the same dc voltage on the falling edge of the clock, the effective voltage across the resistor RSET is a triangular wave going from zero to a positive peak set by the capacitor CSET. Hence the peak current can be set to the desired value by changing the resistor RSET.

The triangular current is mirrored into another branch using a cascode current mirror with a mirroring ratio of 1:20. This current is fed into an H- bridge. The excitation coil of the micro-fluxgate sensor is connected at the output of the H-bridge. The signals H and Hb are applied to the H-bridge such that the direction of current flowing into the excitation coil is reversed on every alternative clock cycle. This results in a 50KHz triangular current being fed to the excitation coil with a peak to peak value twice that of the current drawn from the power supply.

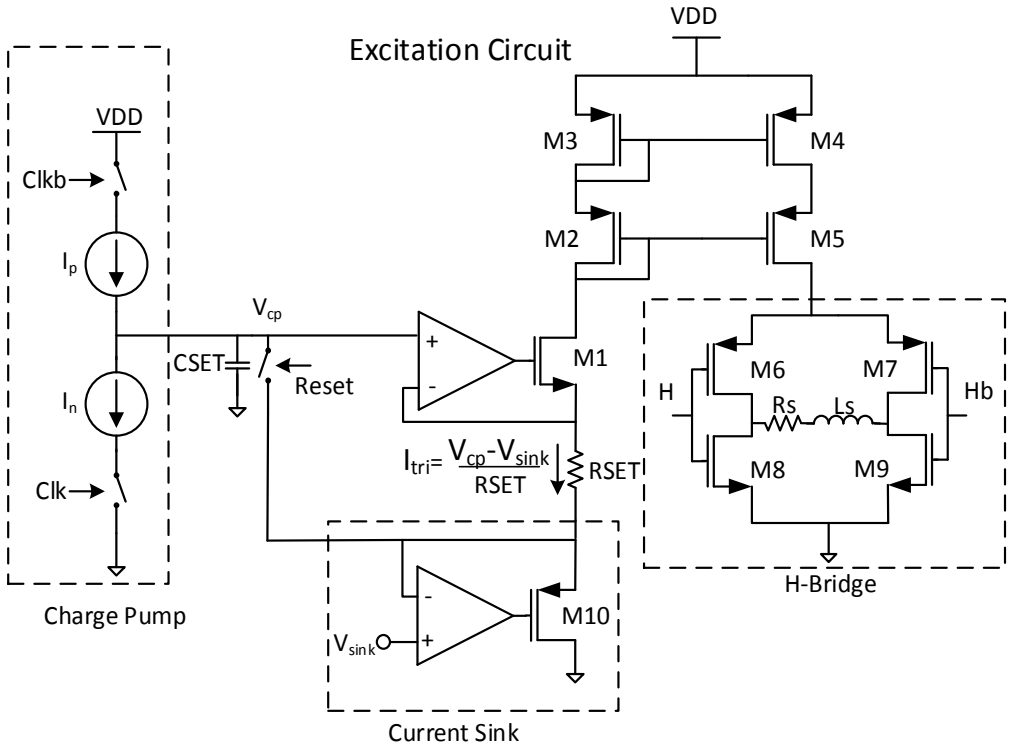

Figure 3.1 Excitation Circuit

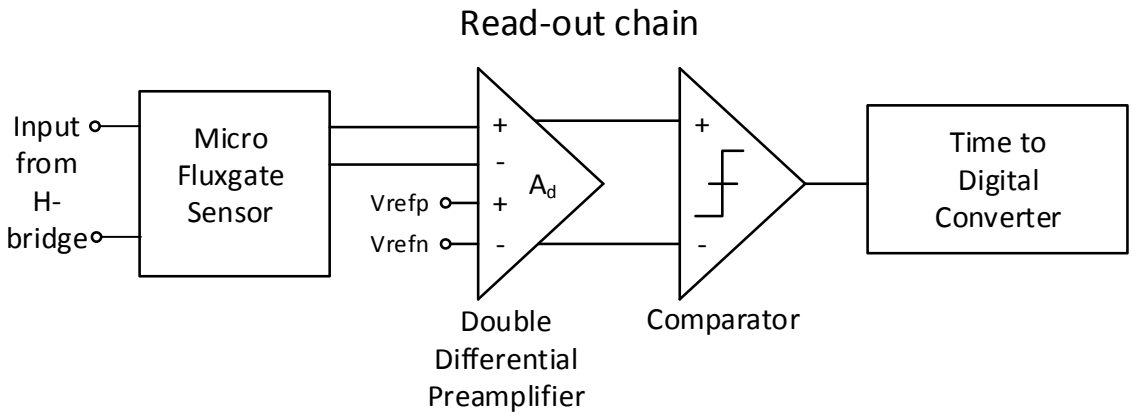

Figure 3.2 Read-out chain

The output of the micro-fluxgate sensor is very low, generally of the order of mV. Hence it has to be amplified before it is fed to a comparator. The read-out chain consists of a double differential preamplifier that amplifies the difference between the output of the sensing coils and a differential reference voltage. This output is of the order of hundreds of mV. The differential output is fed to a comparator that generates a logic high or logic low at its output depending on the inputs.

The output of the comparator remains high for the time period when the differential output voltage of the micro-fluxgate sensor exceeds a certain threshold value set by the differential reference. This corresponds to the time period $\Delta T/2$ as indicated in Figure (1.4). A digital code corresponding to this time is generated by a time to digital converter. The time to digital converter uses a 32MHz crystal clock and its inverted version to generate a digital code of higher resolution which can be generated only by using a 64MHz clock according to the approach used in [19] and [24].

Some of the salient features of the proposed analog front end are:

1) The use of charge pump to generate a triangular voltage waveform gives reduced power consumption compared to previous approaches.
2) H-Bridge is used to switch the direction of current flowing into the excitation coil eliminating the use of symmetric power supply.
3) The read-out circuit is not susceptible to amplitude noise in the output voltage of the sensor.
4) Digital output is produced without using an ADC.
5) The time to digital converter uses a 32MHz clock and generates digital code that is as accurate as the digital code generated using a 64MHz clock using previous approaches in [19] and [24].

3.1 Excitation Circuit

Each block of the excitation circuit is discussed in detail in the following sections.

3.1.1 Charge Pump:

A charge pump consists of two constant current sources which linearly charge or discharge a capacitor at its output. The current sources are connected to the output or disconnected from the output using switches. The charge pump used to generate a triangular voltage waveform is shown in Figure (3.3). The transistors M2 and M3 form a current source that discharges the output and the transistors M4 and M5 form a current source used to charge the output. The transistors M1 and M6 are in triode and are used as switches. The cascode current source formed by M5 and M4 is biased using a wide swing cascode bias with a dummy switch in the bias circuit which replicates the effect of the

switch M6. The cascode current source formed by M2 and M3 is biased using a wide swing cascode bias with a dummy switch in the bias circuit which replicates the effect of the switch M1 [20].

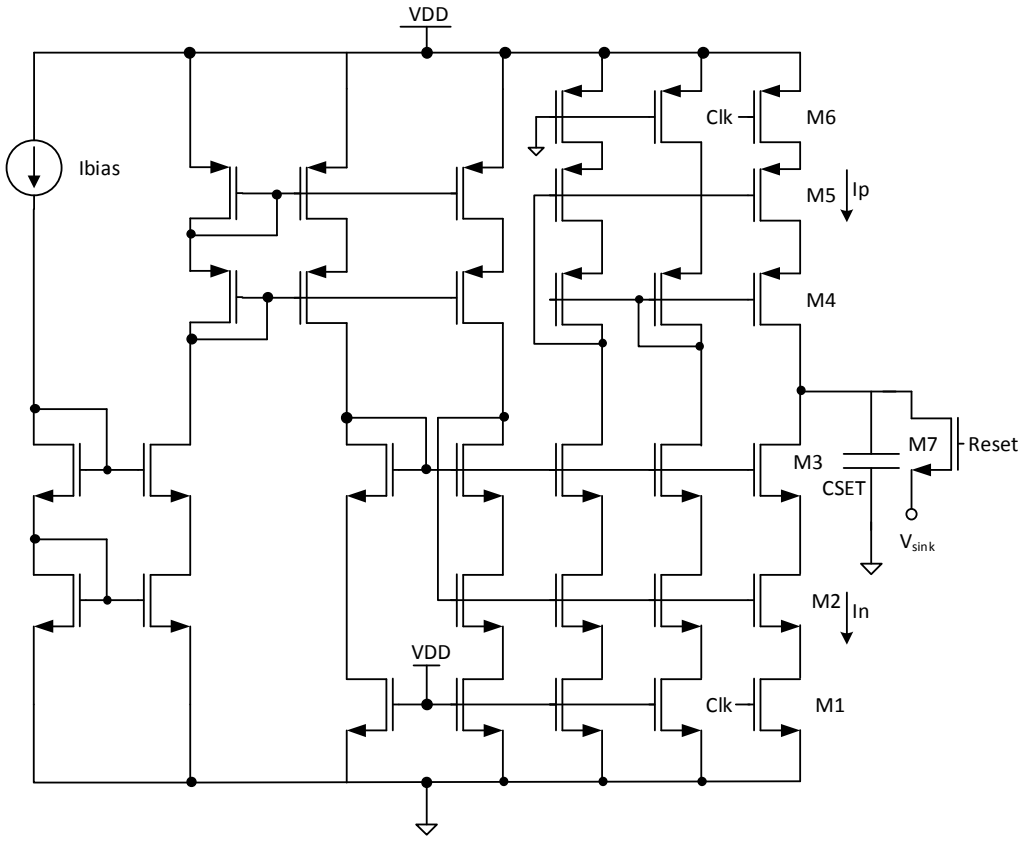

Figure 3.3 Charge Pump

The charge pump shown in Figure (3.3) uses cascode current sources with larger output impedance to reduce the effect of power supply noise on the output. It employs source switching which ensures that the transistors M2-M5 are always in saturation thereby avoiding any peak current that may flow if the transistors M1 and M2 or M4 and M5 are in triode for some portion of time. The switching time for this charge pump is also lower due to the fact that the switches M1 and M6 are connected to a single transistor only.

When the clock goes low the transistor M6 is turned on and M1 is turned off. The output is charged linearly from a voltage V_1 to a peak voltage of V_2 with a charging current of I_p. When the clock goes high the switch M1 is turned on and M6 is turned off. The output is discharged linearly from a voltage V_2 to V_1 with a discharging current of I_n. This is followed by a reset pulse which turns on M7 and resets the output voltage to a value V_{sink} set by the current sink. All the waveforms are shown in Figure (3.4).

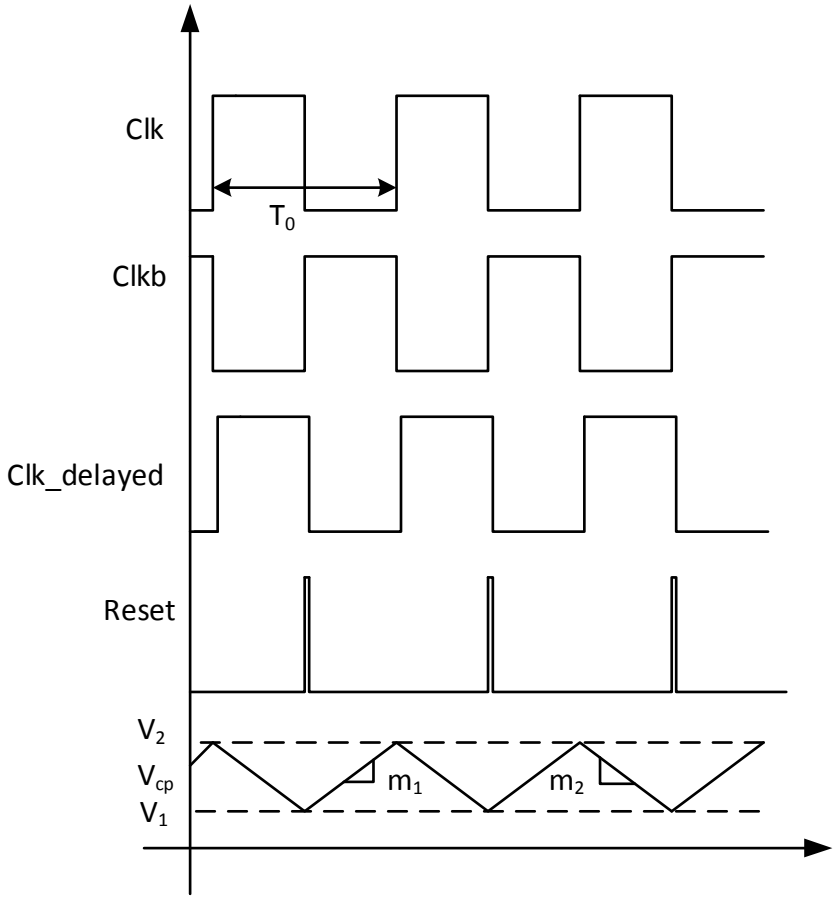

Figure 3.4 Output of Charge Pump

A reset pulse is generated on every falling edge of the clock to reset the output voltage of the charge pump. This is done by delaying the input clock and doing a logical AND operation with the inverted clock. A current starved inverter is used to generate the delayed clock. The schematic is shown in Figure (3.5). The transistors M1 and M4 are in triode where as M2 and M3 are in saturation. When the clock goes low M1 is off and M4 is on. The capacitor C1 is charged linearly to VDD through M3 which acts as a current source. Similarly when clock goes high M1 is on and M4 is off. The capacitor C1 is discharged linearly to ground potential through M2 which acts as a current source. The clock frequency is 100KHz and a reset time of 50ns is used.

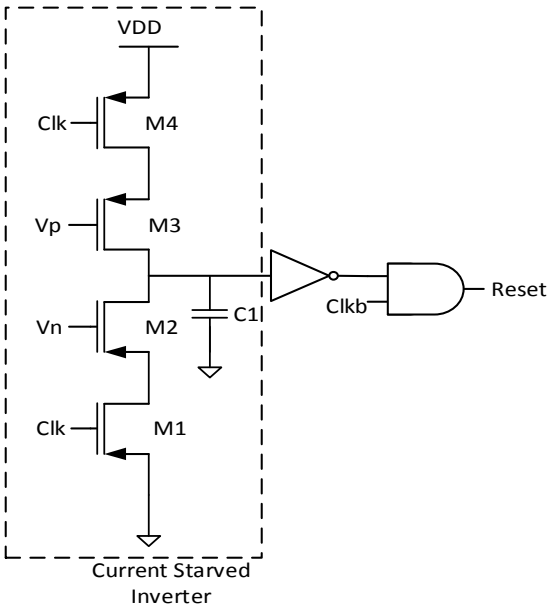

Figure 3.5 Reset Pulse Generation Circuit

The slope of the voltage waveform at the output of the charge pump when the clock is low is:

$$m_1 = \frac{I_p}{CSET} \tag{3.1}$$

The slope of the voltage waveform at the output of the charge pump when the clock is high is:

$$m_2 = \frac{I_n}{CSET} \tag{3.2}$$

If both the charging current and discharging current are equal then

$$I_p = I_n = I_0 \tag{3.3}$$

$$m_1 = m_2 \tag{3.4}$$

$$V_1 = V_{sink} \tag{3.5}$$

$$V_2 = V_{sink} + \frac{I_0}{CSET} * \frac{T}{2} \tag{3.6}$$

If there is a mismatch in the currents I_p and I_n a non-linearity is caused in the voltage at the output of the charge pump when it is reset. Since this happens for a very small amount of time (0.5% of the time period) its effect is very small. There will also be a mismatch in the slopes m_1 and m_2 which modulates the amplitude of the differential sensor output. But since phase delay based read-out is done this will not effect the digital output of the system. The noise in the output voltage of the charge pump due to charge injection from M7 is partly cancelled because it also effects the voltage V_{sink} which subtracted from the voltage at the positive terminal of the resistor RSET as shown in Figure (3.1). The value of I_0 is 5µA and CSET is 40pF.

3.1.2 Triangular Current Generator

The triangular voltage generated at the output of the charge pump is converted into a triangular current using a voltage to current converter. This current is mirrored into another branch using a 1:K current mirror and then flows through the excitation coil of the sensor. The peak value of the mirrored current should be large enough to saturate the magnetic core of the sensor. The schematic of the triangular current generator is shown in Figure (3.6).

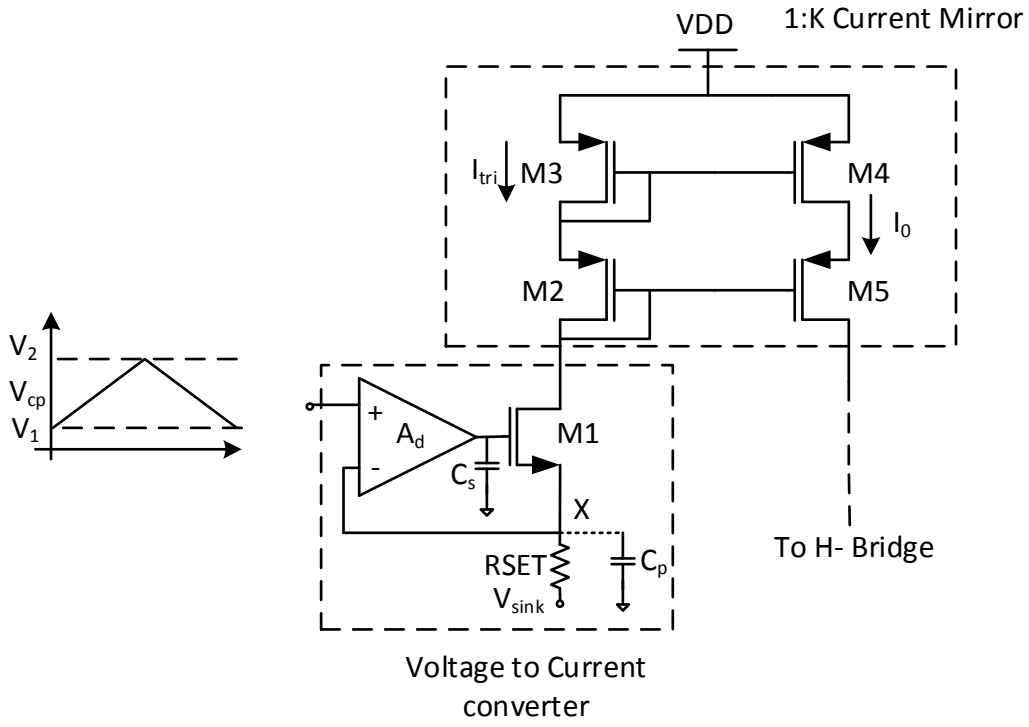

Figure 3.6 Triangular Current Generator

The voltage to current converter applies the triangular voltage across an external resistor through a feedback loop. If the gain of the amplifier A_d is large enough the voltage at the positive terminal of the resistor will be the same as the input voltage from the charge pump. The external resistor sets the current in this branch. It is important that

the excitation current has little variation with temperature so that the output of the sensor is less dependent on temperature. Since the external resistor can be made to have a very good temperature coefficient the current I_{tri} exhibits only a little dependence on temperature. It is also important to have a low offset amplifier so that the voltage across the resistor actually goes from zero to a peak value and so does the current I_{tri}.

$$I_{tri} = \frac{V_{cp} - V_{sink}}{RSET} \tag{3.7}$$

A folded cascode OTA is used to implement the gain stage. The current through the transistor M1 changes from zero to a peak value of few mA. Hence the gate of M1 has to be modulated to supply this wide range of current. So the output of the amplifier should have high swing. The amplifier should have good enough gain so that the voltage at the positive terminal of the resistor RSET is same as the charge pump output voltage. The unity gain bandwidth of the feedback loop should also be large enough to pass a considerable number of harmonics of the input voltage. Since an external resistor is used it will have some parasitic capacitance C_p across it. This forms a pole at a frequency of f_{p2} given by equation (3.8). In order to stabilize the feedback loop the pole at the output of the amplifier, given by equation (3.9), should be the dominant pole. This is done by adding a capacitor C_s at the output of the amplifier.

$$f_{p1} = \frac{1}{2\pi R_{out} * C_s} \tag{3.8}$$

$$f_{p2} = \frac{1}{2\pi R_X * C_p} \tag{3.9}$$

R_{out} is the output impedance of the folded cascode OTA and R_X is the impedance seen at the node X. At higher currents R_x is dominated by the gm of M1 and equals $1/gm_1$. At low currents the gm of M1 decreases and R_x is almost equal to RSET. The capacitance Cs has been chosen such that the feedback loop is stable for all cases. This is verified from the transient response.

The triangular current generated is mirrored into another branch using a 1:K current mirror with K=20. A higher value of K is chosen so as to reduce the bias current. A cascode current mirror is used so as to provide large output impedance. It also helps in reducing the effect of power supply noise on the excitation current. The transistors M2-M5 should be in saturation region for all portion of time. Hence these devices are usually very big and consume a major portion of area. It is important to match the transistors in the current mirror using proper layout techniques as discussed later. Since the resistor RSET is external it can be adjusted to get the required excitation current to saturate the magnetic core. The nominal value of RSET is 230Ω.

3.1.3 Current Sink

The voltage at the negative terminal of the resistance RSET has to be maintained fixed at V_{sink} so that the effective voltage across RSET is a triangular wave going from zero to a certain peak voltage equal to V_2-V_{sink} . And hence the current through the resistor also goes from zero to a peak value linearly. Since the current through this branch is of the order of a few mA the circuit which sinks this current should have extremely low output impedance. A current sink is employed for this purpose.

The schematic of the current sink is shown in Figure (3.7). The impedance looking into the node Y is given as:

$$R_Y = \frac{(1/gm_{10})}{1+A_d} \tag{3.10}$$

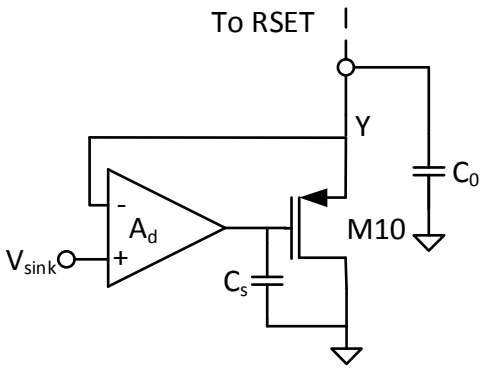

Figure 3.7 Current Sink

A folded cascode OTA followed by a level shifter stage is used for implementing the gain stage. The voltage V_{sink} should be greater than the overdrive voltage of the PMOS transistor M1. Another factor in choosing V_{sink} is the minimum voltage required to be maintained at the output of the charge pump. According to these parameters V_{sink} is set to be 1.5V. The feedback loop has a finite bandwidth and hence an external capacitance of 200pF to ground is used to reduce the variation in the voltage at node Y. The capacitor C_s is added for stability. The folded cascode OTA used here is similar to the one used in the voltage to current converter of triangular current generator. This would reduce the effect of OTA offsets on the excitation current.

3.1.4 H-Bridge

The current supplied by the current mirror is a triangular current that flows from supply to ground through the excitation coil. But the fluxgate sensor needs to be excited with an alternating (AC) current. Hence an H-bridge is used to change the direction of the current through the excitation coil. The schematic of the H-bridge is shown in Figure (3.8).

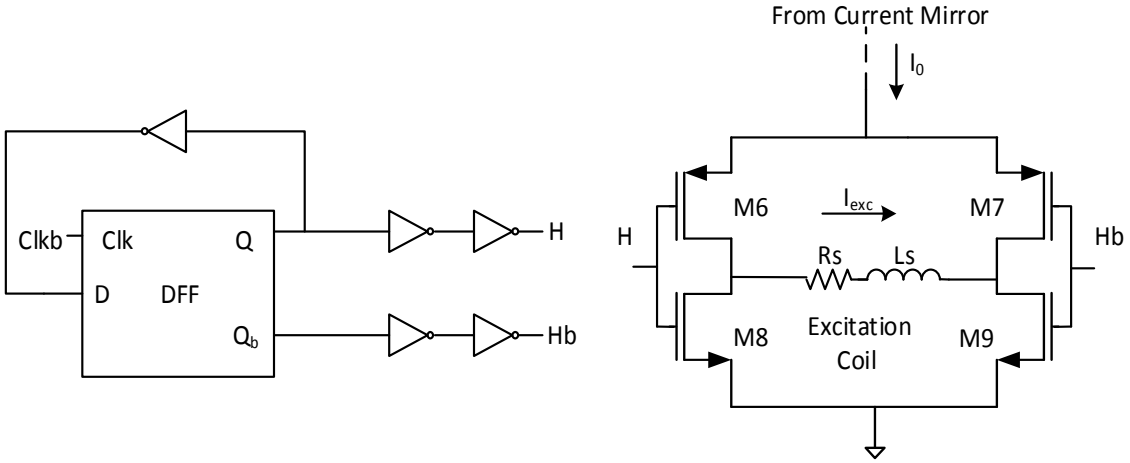

Figure 3.8 H-Bridge Circuit

The H-bridge consists of two CMOS inverter like structures. The current flows in one direction or the other depending on which transistors are turned on. The signals H and Hb which drive the gates of the transistor M6-M9 are should have half of the frequency of the clock that drives the charge pump. Hence a frequency divider with divide by two ratio is used to obtain these signals. The signal H remains high for one clock cycle of the charge pump clock and remains low for the next clock cycle. The signal Hb is an inverted version of the signal H.

When the signal H goes high and Hb goes low, the transistors M7 and M8 are on and the transistors M6 and M9 are off. The current flows through M7- Excitation coil- M8 to ground. In the next clock cycle the H goes low and Hb goes high. Hence the current flows through M6- Excitation coil- M9 to ground. Thus the direction of current flowing through the excitation coil is reversed. The waveforms of various signals in this circuit are shown in Figure (3.9).

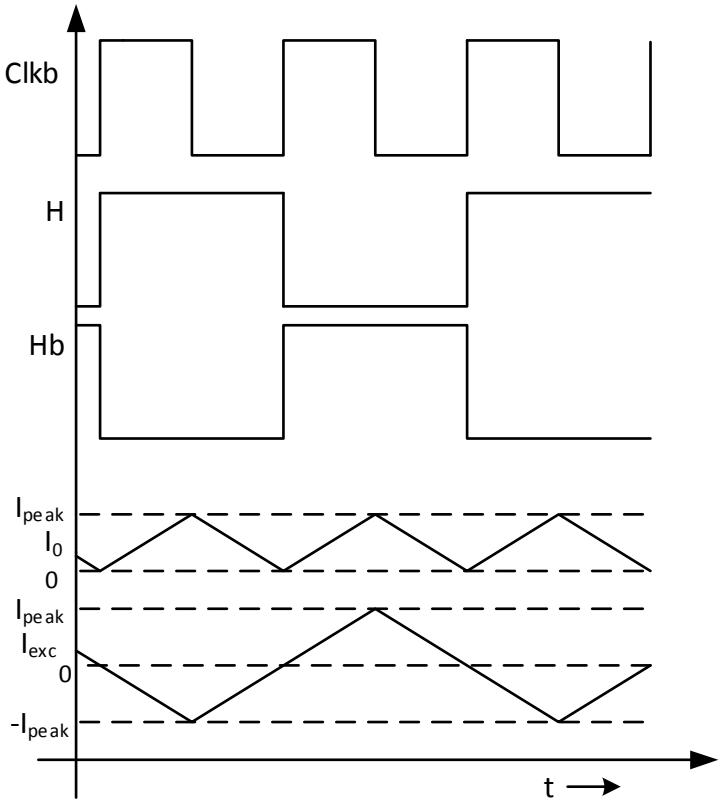

Figure 3.9 Excitation Current Waveforms

The current I_{exc} has a peak to peak value of $2I_{peak}$ but the current drawn from the power supply still has a peak current of I_{peak} only. Since the H-bridge works on current input rather than voltage it has better power supply rejection capability than the 3.3V excitation circuit in [17] which works directly on the supply voltage. The excitation

current will have some spikes at the zero crossings due to the inductive nature of the excitation coil and some parasitic capacitance. This will cause a spike in the voltage at the outputs of individual sensing coils but the differential output voltage will still be clean. This is because all disturbances in the excitation current around zero will appear as common mode noise to the sensor and will be suppressed in the differential output.

3.2 Read-out Chain

In order to measure the phase delay between two consecutive pulses at the output of the fluxgate sensor as described in Chapter 1, we need to process the signals through a triggering circuit like comparator. Micro-fluxgate sensors have noise at the point where the differential output voltage is supposed to be zero. Hence it is desired to have a circuit which is triggered only when the differential voltage exceeds a certain threshold value. The amplitude of the output voltage is usually of the order of mV. Hence it is required to amplify this signal by passing it through a preamplifier before it is given to a comparator. After the comparator a time to digital converter is used to produce an output digital code proportional to the pulse width of the output of the comparator.

3.2.1 Double Differential Preamplifier

The double differential preamplifier forms the first stage of the read-out circuit. The schematic of the double differential preamplifier used is shown in Figure (3.10) [25].

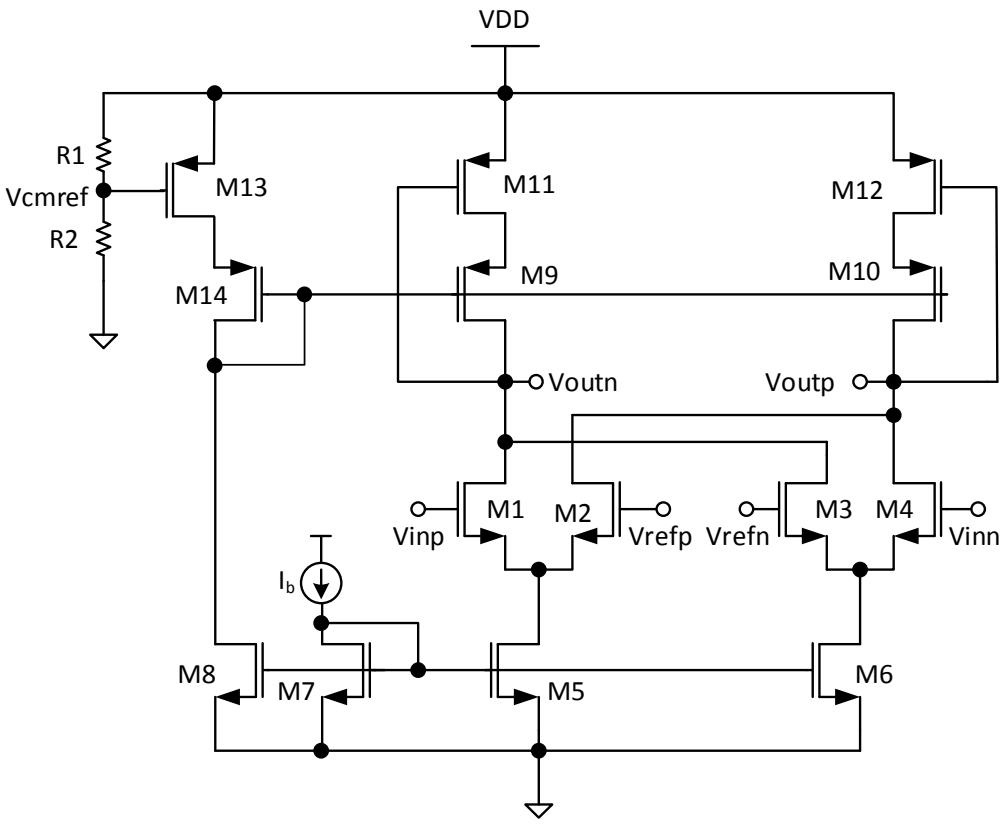

Figure 3.10 Double Differential Preamplifier

The double differential preamplifier is fully differential and gives an output (Voutp-Voutn) which crosses zero when the differential input (Vinp-Vinm) crosses the differential threshold (Vrefp-Vrem). The small signal gain is given as:

$$A_d = gm_1 * (ro_1 || ro_9) \tag{3.11}$$

$$\text{Voutp-Voutn} = A_d((\text{Vinp-Vinn})-(\text{Vrefp-Vrefn})) \tag{3.12}$$

In order to obtain a good gain active load is used in the preamplifier. This necessitates the use of Common Mode Feedback (CMFB) to set the output dc level reliably. The transistors M11-M13 are in triode. The resistance of these transistors is

adjusted such that ID9 and ID10 exactly balance ID5 and ID6 respectively. If we assume that the (W/L) of M14 is equal to the (W/L) of M9 and M10 then the currents through all of these transistors will be equal. Hence if (W/L) of M13 equals the (W/L) of M11 and M12 the currents ID14 and ID9, 10 track each other. This sets the output common mode equal to Vcmref. In practice Vds of M14 and M9 are not equal and this would result in a finite error. The output swing is also limited by the transistors M11 and M12 as the output voltage cannot go beyond VDD-$|V_{th11,12}|$. But these two limitations do not have a major effect on the current read- out circuit.

$$\text{Vcmref}=\frac{R_2}{R_1+R_2}\text{VDD} \tag{3.13}$$

$$\text{Voutdc}=\left(\frac{\text{Voutp}+\text{Voutn}}{2}\right) \tag{3.14}$$

$$\text{Voutdc}=\text{Vcmref if}\left(\frac{W}{L}\right)_{13}=\left(\frac{W}{L}\right)_{11,12}\text{and}\left(\frac{W}{L}\right)_{14}=\left(\frac{W}{L}\right)_{9,10} \tag{3.15}$$

It is important to have good matching between the input devices to have low offsets. However offsets less than a mV do not have a significant impact because the output of the sensor has a relatively small rise time.

3.2.2 Comparator

The output of the preamplifier is of the order of a few hundred mV. This is given as input to a comparator stage which produces proper logic levels at it its output. The comparator used in the read- out circuit is shown in Figure (3.11) [20].

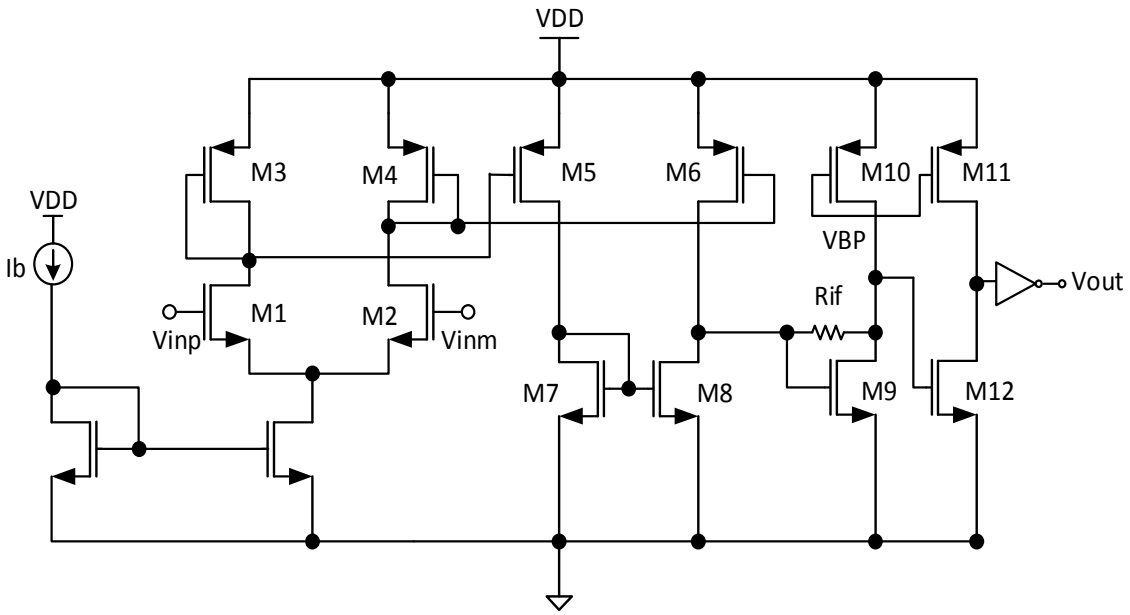

Figure 3.11 Current-mode Comparator

The comparator is a current mode comparator. Current mode comparators have higher speed and larger bandwidth. They also require lower voltage headroom to operate than those operating in voltage mode. The comparator consists of a transconductance stage followed by a current subtractor, two current-source inverting amplifiers and a CMOS inverter. The differential input voltage produces a proportional difference in the currents flowing through the transistors M1 and M2. These currents are mirrored into M5 and M6. The difference in the currents through M6 and M5 flows into the first current source amplifier. The first current-source amplifier employs resistive feedback to reduce the input and output impedances. The signal is passed through another current-source amplifier and a CMOS inverter to produce a signal with proper logic levels at the output.

3.2.3 Time to Digital Converter

The output of the comparator has a certain pulse width with proper logic levels. A digital word corresponding to this pulse width is produced by a time to digital converter. Conventional fluxgate sensors have very low excitation frequencies of the order of Hz and hence a counter run at a few tens of MHz would give good resolution. Micro-fluxgate sensors have excitation frequencies of the order of few hundreds of kHz. Hence time to digital converter also forms a crucial part of the read-out chain.

The time to digital converter used is shown in Figure (3.12). It uses two synchronous counters which run on a 32MHz clock and its inverted version. The output of the comparator is given as an enable to the counters. When enable goes high both the counters start counting. When the enable goes low the counters retain the count. After this the Latch signal goes high for one clock cycle of the 32MHz clock. The data in the counters is latched into a bank of D Flip-flops. The Latch signal is followed by reset signal which resets the counters. The digital codes in the D Flip-flops are added using an 8-bit adder. The resulting code corresponds to the pulse width of the output of the comparator and hence is proportional to the external magnetic field. For each enable pulse the digital code is updated.

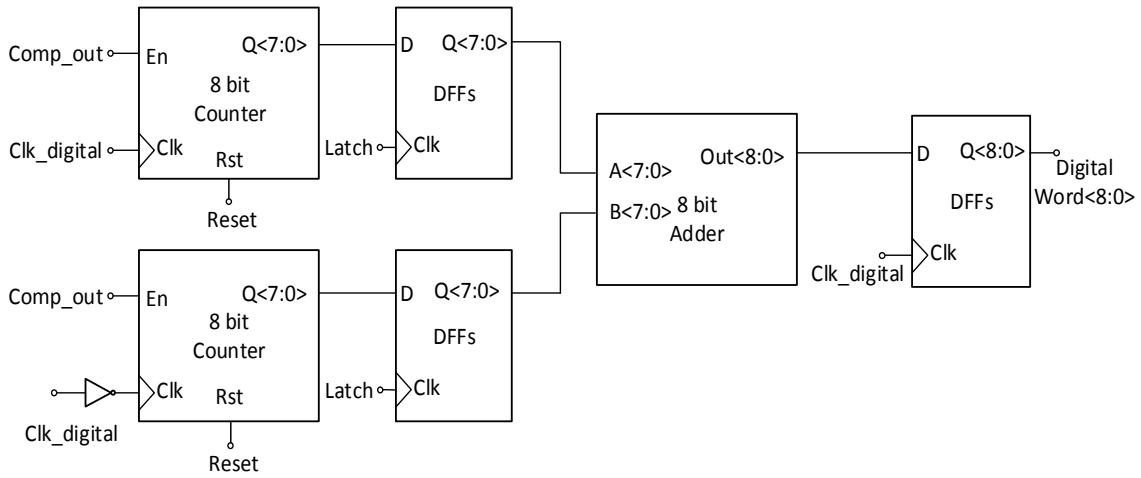

Figure 3.12 Time to Digital Converter

The waveforms of various signals are shown in Figure (3.13). The advantage of using two counters is that we can get one bit more resolution in the time to digital conversion process. The resolution of the time to digital converter is now 15.625ns. With the approach used in [19] and [24] it would take a 64MHz clock to produce data with this resolution.

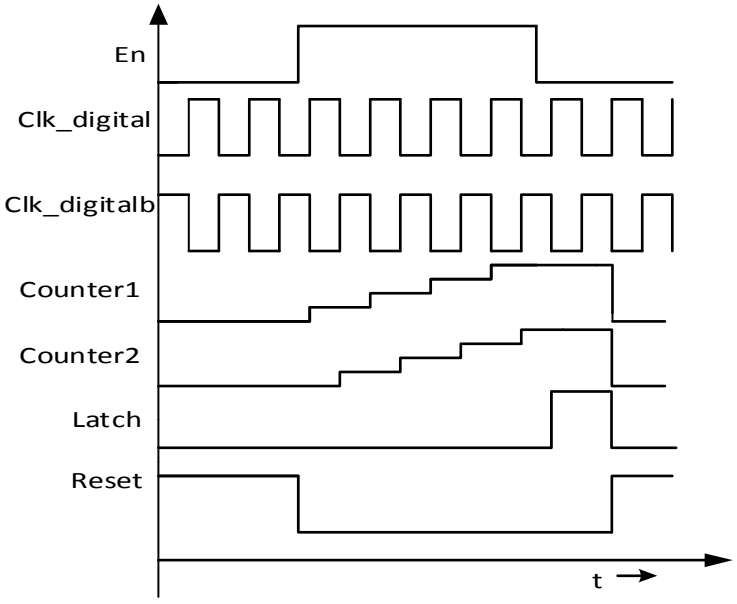

Figure 3.13 Time to Digital Converter waveforms

3.3 Layout

The layout of the excitation circuit, double differential preamplifier and comparator is done in IBM 0.18µm CMHV7SF process using the high voltage MOSFETs. A snapshot of the layout is shown in Figure (3.14).

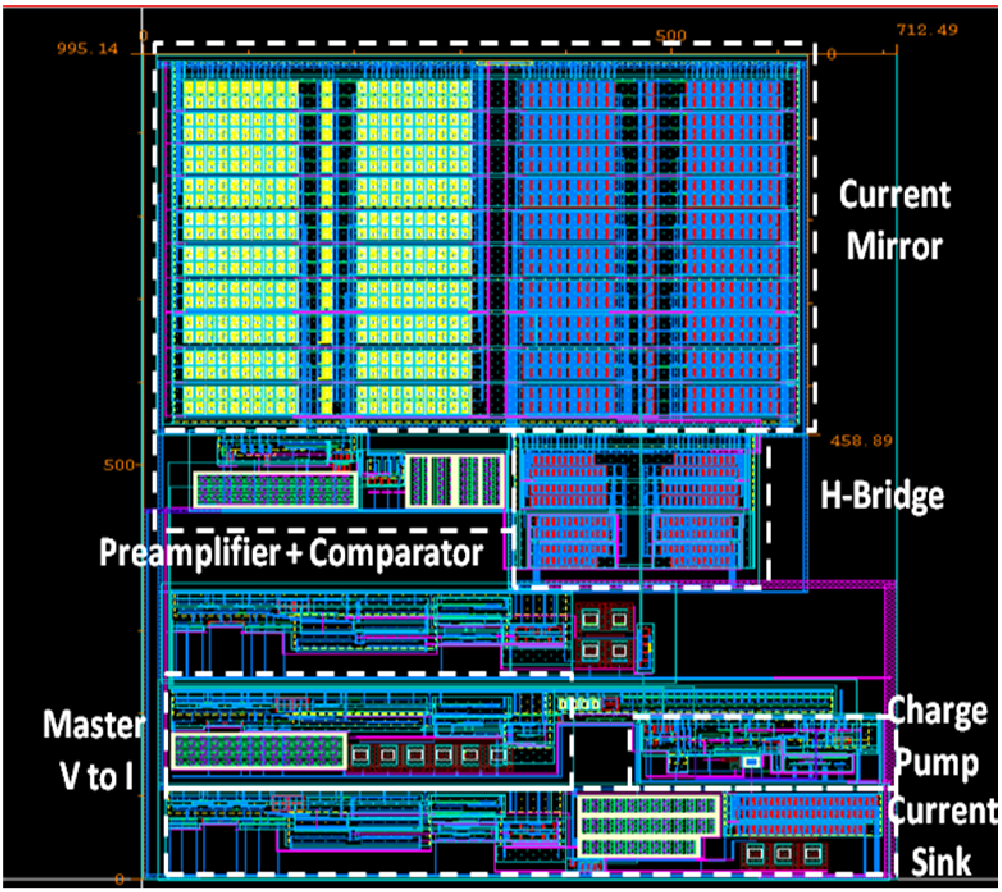

Figure 3.14 Layout of Analog Front-End Circuit

The area of the layout is 995.14*712.49µm^2. Current mirror occupies a major portion of the area. Separate power supply and ground pins are used for the current mirror and H-bridge since they work at higher currents. Common centroid and interdigitation techniques are used to get good matching between devices whenever it is necessary.

Chapter 4

RESULTS

The results of post layout extracted simulations are presented in this section. Parasitic resistance, capacitance and coupling capacitance are extracted using R-C-Cc extraction. The charge pump output voltage is shown in Figure (4.1).

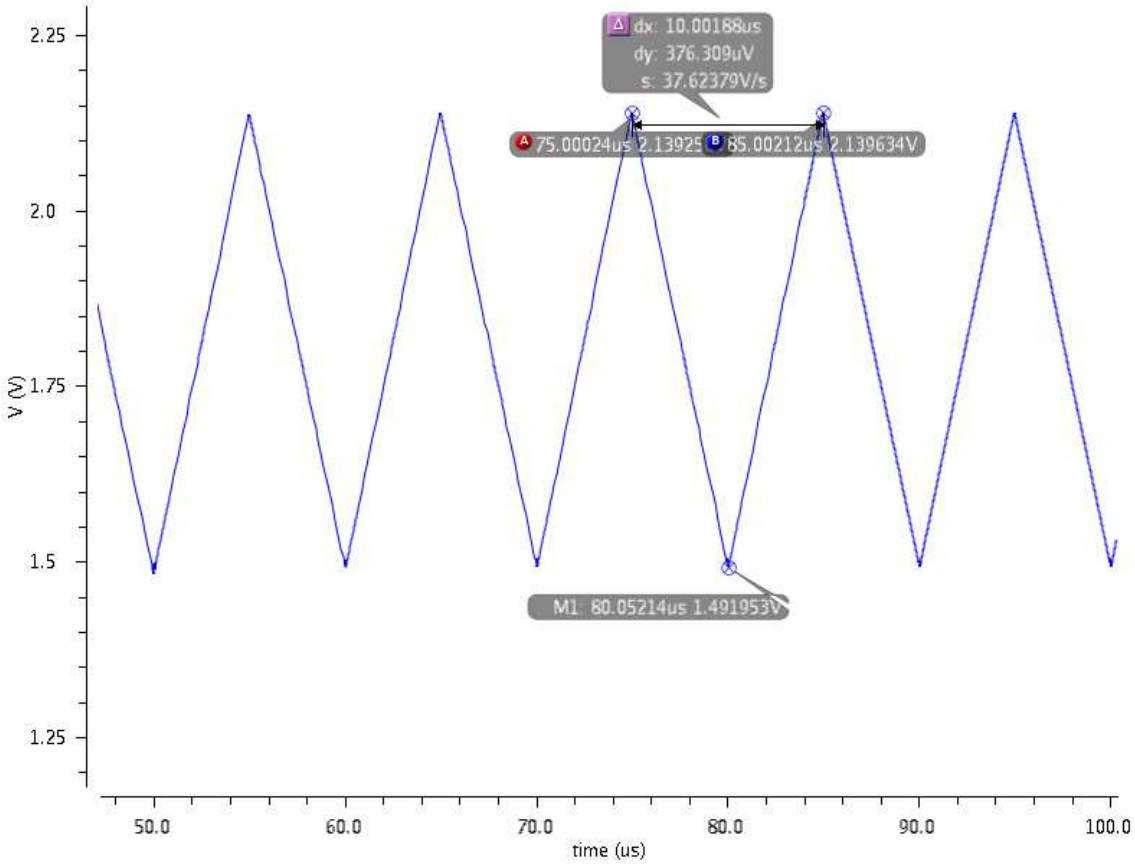

Figure 4.1 Charge Pump Output Voltage

The peak to peak value of the triangular voltage is 647.65mV and it has a frequency of 100KHz.

The excitation current waveforms are shown in Figure (4.2). The current goes above 50mA and below -50mA which is the current required to saturate the core. It has a frequency of 50 KHz.

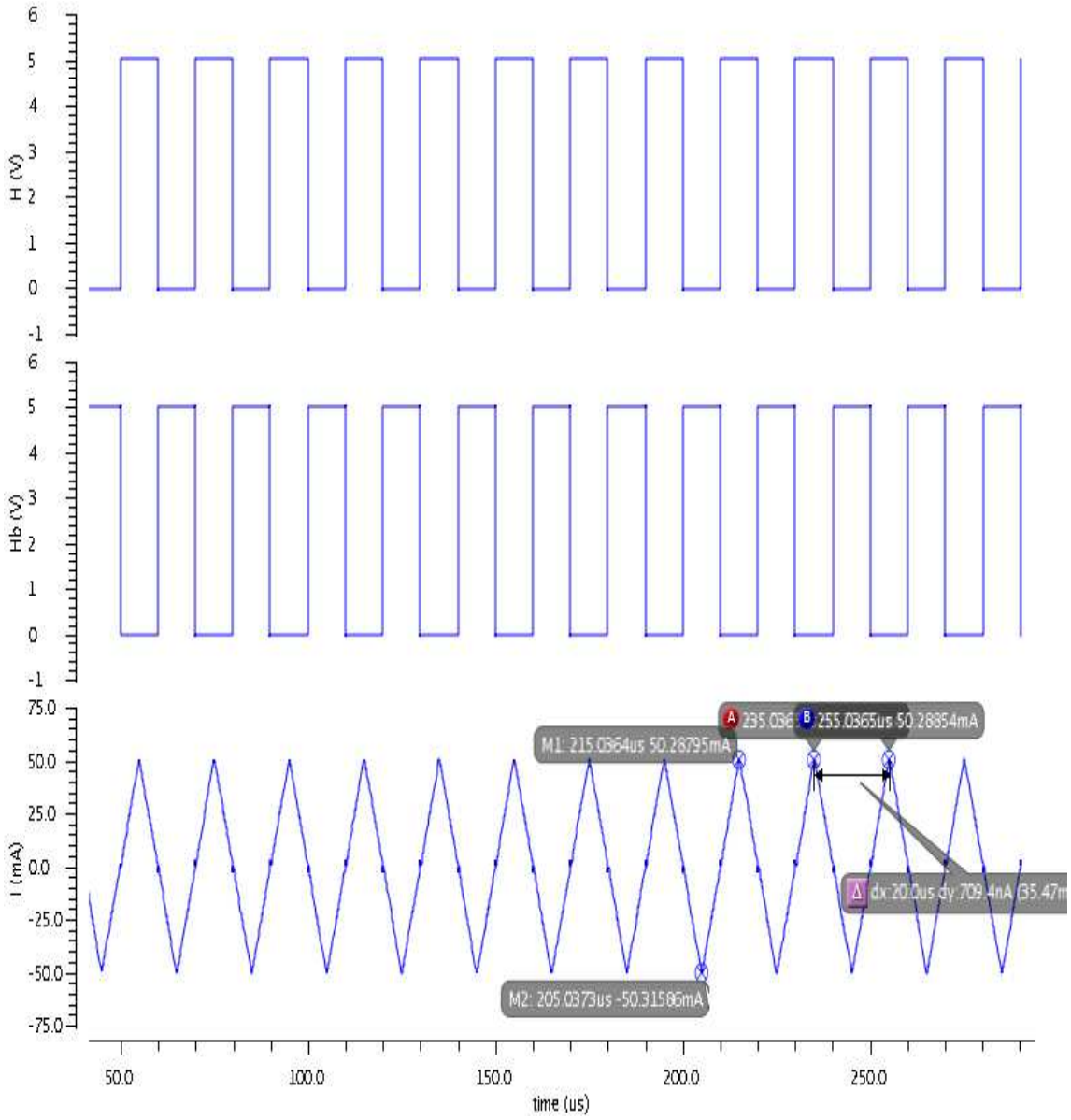

Figure 4.2 Excitation Current Waveform

The differential output of the sensor is shown in Figure (4.3). The peak to peak value is around 30mV.

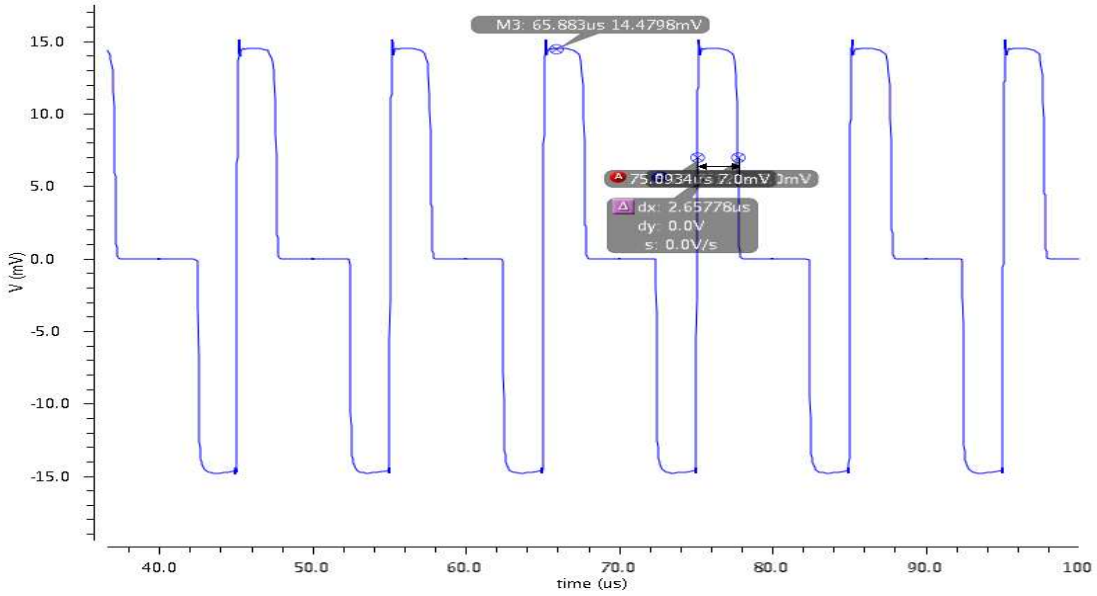

Figure 4.3 Output of Micro-Fluxgate Sensor

The pulse width at the output of the sensor and comparator is shown in Figure (4.4).

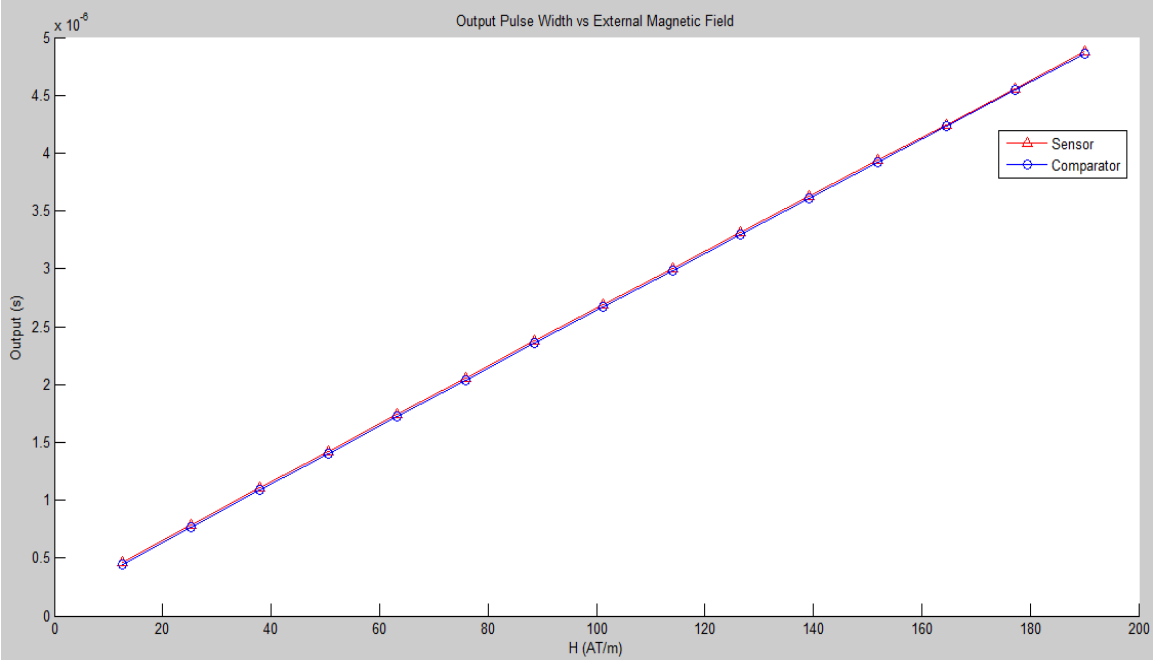

Figure 4.4 Output of Sensor and Comparator vs External Magnetic Field

The difference between the outputs of sensor and comparator is shown in Figure (4.5).

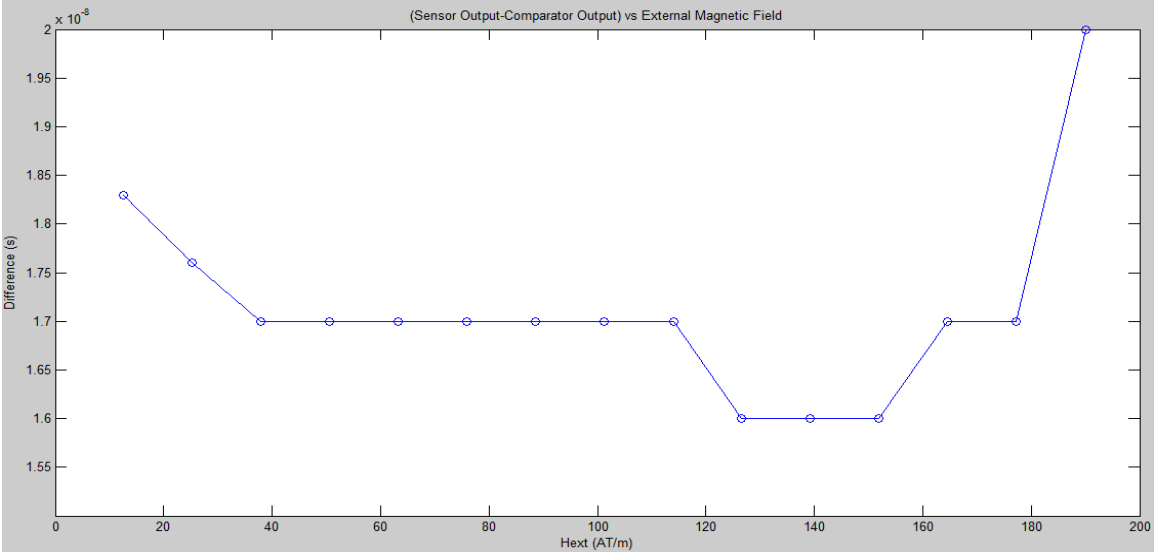

Figure 4.5 Difference between Sensor and Comparator Output vs External Magnetic field

It can be seen that the difference is almost constant at 17ns and changing by ± 1ns. The non-linearity caused by the comparator is therefore very low. The percentage linearity error vs external magnetic field is shown in Figure (4.6).

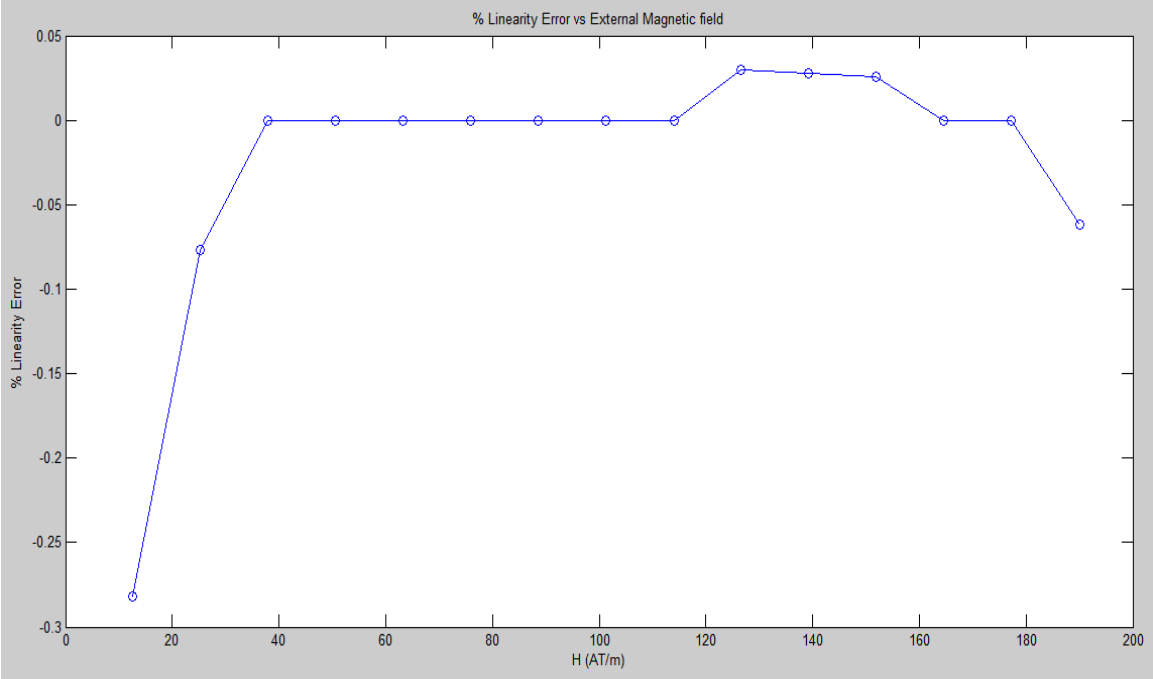

Figure 4.6 %Linearity Error vs External Magnetic Field

The digital output of the system vs external magnetic field is shown in Figure (4.7).

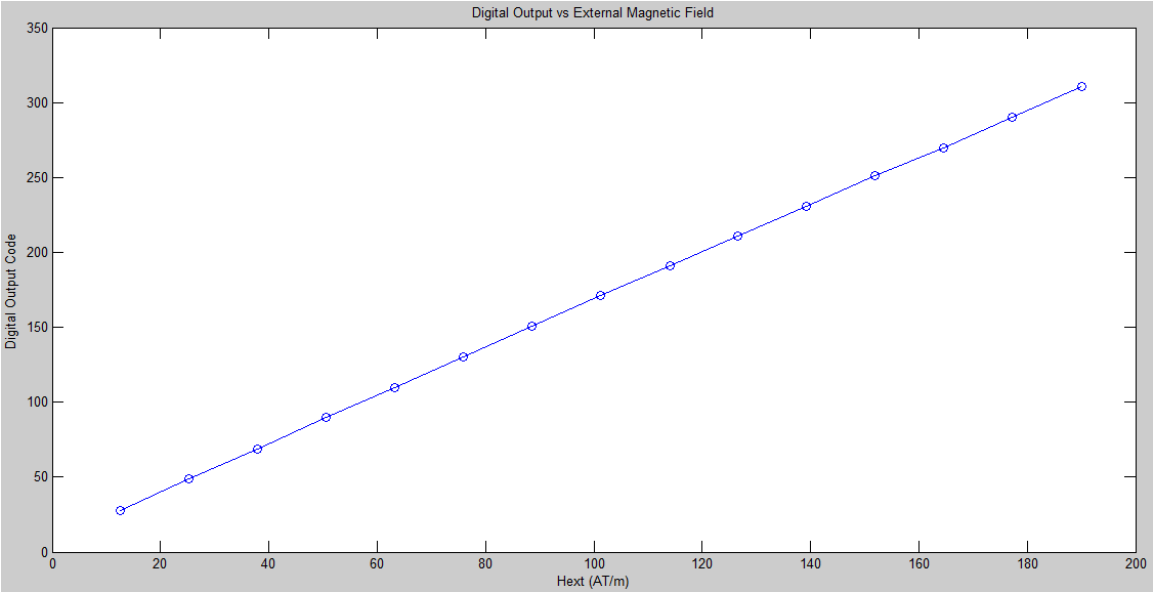

Figure 4.7 Digital Output vs External Magnetic Field

Table 3.1 summarizes the key specifications of the developed analog front-end circuit.

Parameter	**Value**
Process	IBM CMOS 0.18µm
RMS Power Consumption of AFE (excludes the power delivered to the sensor)	5.025mW
%Linearity Error at the output of comparator	-0.282%
Resolution of time to digital converter	15.625ns with 32MHz clock
Layout area	995.14*712.49µm^2

Table 4.1 Key Specifications of Developed Analog Front-End

Chapter 5

CONCLUSION

A new analog front-end circuit for micro-fluxgate sensors is developed. Charge pump based excitation circuit is used to reduce the power consumption of the excitation circuit. An H-bridge is used to reverse the direction of current through the excitation coil without the use of symmetric power supply. Phase delay based read-out technique is implemented. It produces a digital output without using an ADC. The read-out circuit is immune to amplitude noise and hence it is best suited for use for micro-fluxgate sensors whose output voltage is much lower. Phase delay based read-out circuit also has low power.

The analog front-end circuit is simulated with a SPICE model of micro-fluxgate sensor and excellent linearity in the output is obtained. An offset of about 17ns is produced at the output due to asymmetric rise and fall times at the output of the sensor. But it can be easily calibrated. The time to digital converter produces an output with 15.625ns resolution using a 32MHz clock. The analog front end circuit consumes 5.025mW of power excluding the power supplied to the micro-fluxgate sensor and the bias current to the current mirror. This is much lower compared to the power consumption of the state-of-the-art analog front end circuits presented in this thesis. The layout has an area of 995.14*712.49μm^2. The area can be further reduced depending on the current consumption of the sensor.

REFERENCES

[1] Pavel Ripka, Advances in fluxgate sensors, Sensors and Actuators A: Physical, Volume 106, Issues 1–3, 15 September 2003

[2] Velasco-Quesada, G.; Román-Lumbreras, M.; Conesa-Roca, A.; Jeréz, F., "Design of a Low-Consumption Fluxgate Transducer for High-Current Measurement Applications," *Sensors Journal, IEEE* , vol.11, no.2, pp.280,287, Feb. 2011

[3] Florian Kaluza, Angelika Grüger, Heinrich Grüger, New and future applications of fluxgate sensors, Sensors and Actuators A: Physical, Volume 106, Issues 1–3, 15 September 2003

[4] Major, R. V., "Current measurement with magnetic sensors," *Magnetic Materials for Sensors and Actuators (Digest No. 1994/183), IEE Colloquium on* , vol., no., pp.5/1,5/3, 11 Oct 1994

[5] Baschirotto, A.; Dallago, E.; Malcovati, P.; Marchesi, M.; Venchi, G., "From a PCB Fluxgate to an integrated micro Fluxgate magnetic sensor," *Instrumentation and Measurement Technology Conference, 2005. IMTC 2005. Proceedings of the IEEE* , vol.3, no., pp.1756,1760, 16-19 May 2005

[6] Baschirotto, A.; Dallago, E.; Malcovati, P.; Marchesi, M.; Venchi, G., "Fluxgate magnetic sensor in PCB technology," *Instrumentation and Measurement Technology Conference, 2004. IMTC 04. Proceedings of the 21st IEEE* , vol.2, no., pp.808,812 Vol.2, 18-20 May 2004

[7] Baschirotto, A.; Dallago, E.; Ferragina, V.; Ferri, M.; Grassi, M.; Malcovati, P.; Marchesi, M.; Melissano, E.; Morelli, M.; Rossini, A.; Ruzza, S.; Siciliano, P.; Venchi, G., "A CMOS 2D Micro-Fluxgate Earth Magnetic Field Sensor with Digital Output," *Solid-State Circuits Conference, 2007. ISSCC 2007. Digest of Technical Papers. IEEE International* , vol., no., pp.390,610, 11-15 Feb. 2007

[8] Jian Lei, Chong Lei, Yong Zhou, Fabrication and characterization of a new MEMS fluxgate sensor with nanocrystalline magnetic core, Measurement, Volume 45, Issue 3, April 2012

[9] Maria Teresa Todaro, Leonardo Sileo and Massimo De Vittorio (2012). Magnetic Field Sensors Based on Microelectromechanical Systems (MEMS) Technology, Magnetic Sensors - Principles and Applications, Dr Kevin Kuang (Ed)

[10] Ripka, P. (2001). *Magnetic sensors and magnetometers*. Boston: Artech House

[11] Go□pel, W., J. Hesse, J. N. Zemel, R. Boll, and K. J. Overshott. 1989. *Sensors: a comprehensive survey Vol. 5, Vol. 5*. Weinheim: VCH

[12] Gupta, S.; Ahn, Chong H.; Park, J., II, "Electromagnetic modeling and harmonic analysis of micro-machined ring-type magnetic fluxgate sensor using SPICE," *Sensors, 2003. Proceedings of IEEE* , vol.1, no., pp.622,625 Vol.1, 22-24 Oct. 2003

[13] Gupta, Sukirti. "Simulation and Optimization of Micromachined Magnetic Fluxgate Sensors." Electronic Thesis or Dissertation. University of Cincinnati, 2002

[14] Ripka, P.; San On Choi; Tipek, A.; Kawahito, S.; Ishida, M., "Pulse excitation of micro-fluxgate sensors," *Magnetics, IEEE Transactions on* , vol.37, no.4, pp.1998,2000, Jul 2001

[15] Baschirotto, A.; Borghetti, F.; Dallago, E.; Malcovati, P.; Marchesi, M.; Venchi, G., "A CMOS front-end circuit for integrated fluxgate magnetic sensors," *Circuits and Systems, 2006. ISCAS 2006. Proceedings. 2006 IEEE International Symposium on* , vol., no., pp.4 pp.,4406, 21-24 May 2006

[16] Baschirotto, A.; Dallago, E.; Malcovati, P.; Marchesi, M.; Melissano, E.; Morelli, M.; Siciliano, P.; Venchi, G., "An Integrated Micro-Fluxgate Magnetic Sensor With Front-End Circuitry," *Instrumentation and Measurement, IEEE Transactions on* , vol.58, no.9, pp.3269,3275, Sept. 2009

[17] Ferri, M.; Surano, A.; Rossini, A.; Malcovati, P.; Dallago, E.; Baschirotto, A., "Low-voltage fluxgate magnetic current sensor interface circuit with digital output for portable applications," *Sensors, 2009 IEEE* , vol., no., pp.79,82, 25-28 Oct. 2009

[18] R Gottfried-Gottfried, W Budde, R Jähne, H Kück, B Sauer, S Ulbricht, U Wende, A miniaturized magnetic-field sensor system consisting of a planar fluxgate sensor and a CMOS readout circuitry, Sensors and Actuators A: Physical, Volume 54, Issues 1–3, June 1996

[19] P.D Dimitropoulos, J.N Avaritsiotis, E Hristoforou, Boosting the performance of miniature fluxgates with novel signal extraction techniques, Sensors and Actuators A: Physical, Volume 90, Issues 1–2, 1 May 2001

[20] Woogeun Rhee, "Design of high-performance CMOS charge pumps in phase-locked loops," *Circuits and Systems, 1999. ISCAS '99. Proceedings of the 1999 IEEE International Symposium on* , vol.2, no., pp.545,548 vol.2, Jul 1999

[21] Byung-Moo Min; Soo-Won Kim, "High performance CMOS current comparator using resistive feedback network," *Electronics Letters* , vol.34, no.22, pp.2074,2076, 29 Oct 1998

[22] Marchesi, M.: Fluxgate Magnetic Sensor System for Electronic Compass, Dissertation, Universita' Degli Studi di Pavia

[23] Ferri, M.:Integrated magnetic sensor interface circuits and photovoltaic energy harvester systems, Dissertation, Universita' Degli Studi di Pavia

[24] Baglio, S.; Sacco, V.; Bulsara, A., "Read-out circuit in RT-fluxgate," *Circuits and Systems, 2005. ISCAS 2005. IEEE International Symposium on* , vol., no., pp.5910,5913 Vol. 6, 23-26 May 2005

[25] Razavi, Behzad. "Design of Analog CMOS Integrated Circuits."